Title

Poly (Lactic-co-Glycolic Acid)-Polyethylene Glycol Nanoparticles for Therapeutic Delivery to Traumatic Brain Injury

Author

North, Katherine Mackenzie

Publication Date

2021

Peer reviewed|Thesis/dissertation

UNIVERSITY OF CALIFORNIA SAN DIEGO

Poly (Lactic-co-Glycolic Acid)-Polyethylene Glycol Nanoparticles for Therapeutic Delivery to Traumatic Brain Injury

A thesis submitted in partial satisfaction of the requirements for the degree Master of Science

In

Bioengineering

By

Katherine Mackenzie North

Committee in charge:

Professor Ester J. Kwon, Chair
Professor Karen L. Christman
Professor Sameer B. Shah

2021

The Thesis of Katherine Mackenzie North is approved, and it is acceptable in quality and form for publication on microfilm and electronically.

University of California San Diego

2021

DEDICATION

This thesis is dedicated to my Mom and Dad, who have always supported me through school and encouraged me to go on every adventure, especially this one.

To my loving sister Kylie, who always inspires me to be the best individual I can be and always push past my limitations to reach new heights.

To Elizabeth Hyde and Rhys Roberts, without whom this thesis would not exist. You are the best friends I could ever have.

Finally, thank you to everyone who has helped me get to this point.

EPIGRAPH

And you may ask yourself, how did I get here?

And you may tell yourself,

This is not my end.

And you may tell yourself,

This is just my beginning.

Table of Contents

List of Abbreviations

BBB – Blood-Brain Barrier

CCI – Controlled Cortical Impact

CNS – Central Nervous System

DCM – Dichloromethane

DLS – Dynamic Light Scattering

EE – Encapsulation Efficiency

EPR – Enhanced Permeability and Retention

FDA – Food and Drug Administration

GCS – Glasgow Coma Scale

LC – Loading Capacity

PBS – Phosphate-buffered saline

PEG – Polyethylene Glycol

PLGA – Poly(Lactic-co-Glycolic Acid)

PVA –Polyvinyl Alcohol

MW – Molecular Weight

NAC – N-Acetylcysteine

Nps – Nanoparticles

RES – Reticuloendothelial system

ROI – Region of Interest

ROS – Reactive Oxygen Species

SCI – Spinal Cord Injury

TBI –Traumatic Brain Injury

List of Figures

List of Schemes

Acknowledgments

I would like to express my most profound appreciation to my committee chair, Professor Ester J. Kwon, who has the wisdom and kindness of a great mentor: she has continually conveyed a spirit of adventure regarding research and scholarship and excitement about teaching. Without her guidance and persistent help, this thesis would have been impossible.

I would like to thank my committee members, Professor Karen L. Christman and Professor Sameer B. Shah, whose intelligence demonstrated to me the need for thoughtful design throughout the entire process of nanoparticle development.

In addition, an immense thank you to Ph.D. student Rebecca Kandell who provided guidance and assistance throughout the entire process of my Master's degree here at UCSD. Rebecca has a personality that can light up the whole room. She can manage to cheer you up when nothing in Lab is going right, and she was an absolute joy to work with. I will miss you greatly as I move on to the next phase in my career.

ABSTRACT OF THE THESIS

Poly (Lactic-co-Glycolic Acid)-Polyethylene Glycol Nanoparticles for Therapeutic Delivery to Traumatic Brain Injury

by

Katherine Mackenzie North

Master of Science in Bioengineering

University of California San Diego, 2021

Professor Ester J. Kwon, Chair

Traumatic brain injury (TBI) presents a severe challenge for modern medicine due to the poor regenerative capabilities of the brain, complex pathophysiology, and lack of effective treatment for TBI to date. The overall goal of this research is to develop a nanoparticle capable

of sustained drug release for the delivery and treatment of TBI so that therapeutic drugs can be delivered after the Blood-Brain Barrier (BBB) closes 24 hours after injury. Poly(lactic-co-glycolic acid) (PLGA) nanoparticles have shown some experimental success; yet, none have yielded improved clinical efficacy results. Polyethylene Glycol (PEG) has been shown to act as a stealth molecule that can increase the circulation time of particles. In addition, N-acetylcysteine has demonstrated neuroprotective and anti-inflammatory potential. This paper presents the development of PEGylated PLGA NPs synthesized using double and single emulsion for potential therapeutic delivery to TBI. Dynamic light scattering (DLS) shows PEG-PLGA NPs to have an average diameter of 200 nm. Loading capacity was obtained at 2%, and drug encapsulation efficiency was obtained at 55%. A biphasic drug release pattern was observed in situ, and drug release was assessed in vitro over 72 h using FRET nanoparticles; almost complete drug release was seen during this time. Finally, in vivo administration of PEG-PLGA NPs demonstrated that PEGylated NPS were able to show reduced accumulation in filtration organs such as the liver and kidneys compared to bare PLGA particles. This evidence supports the potential of PEG-PLGA NPs as a promising carrier to develop TBI therapeutics.

Introduction

1.1 Motivation

Traumatic Brain Injury (TBI) is a leading cause of death and disability among children and young adults in the United States [1]. TBI has earned itself the "silent epidemic" nickname due to its precedence as a growing public health crisis. Most problems experienced by those suffering from TBI, such as impairments to cognitive ability and memory faction, are invisible to those not affected [2]. It is estimated that globally roughly 69 million people are affected annually by some form of TBI [3]. In the US alone, the most recent surveillance report on TBI from the CDC found that approximately 2.87 million cases of TBI-related emergency department visits and hospitalizations were reported in 2014. Eight hundred thirty-seven thousand of those reported cases occurred among children, and 56,800 reports resulted in death [4]. It is estimated that an additional 80,000 to 90,000 of those individuals to sustain a TBI injury also sustain long-term disability from the original trauma [1]. As the cumulative result of past TBI, an estimated 5.3 million people live with a permanent TBI-related disability in the United States today. The lifetime economic burden is estimated to be approximately $76.5 billion as of 2010 [1]. With the three leading causes of TBI being motor vehicle crashes, violence, and falls, it is expected that the global impact of TBI will only increase in future years. Road traffic accidents are currently ranked as the ninth leading cause of death globally and are projected to rise to fifth place by 2030, going from 1.3 million accidents per year as of 2004 to 2.4 million [5]. Additionally, with the global incidence rate of suicide attempts increasing steadily, there has also been a notable increase in TBI-related deaths due to intentional self-harm, rising 17% from 2006-2014, making it the fastest-

growing cause for TBI [4]. With the reported cases of TBI increasing each year and the immense impact on patient quality of life and loss of productive years to consider, therapeutic treatment options that improve the long-term brain health of TBI patients are desperately needed.

1.2 Background

1.2.1 Traumatic Brain Injury

Traumatic Brain Injury (TBI) is caused by an external force to the head that disrupts the typical structure and physiology of the brain [6]. This force can take the form of a direct impact to the skull, rapid acceleration-deceleration, or even the force of a blast wave. However, the most predominant causes of TBI include blunt force trauma or penetrating wound to the head after a traffic accident, falls, gunshot wounds, and assault [7], [8]. TBI has a biphasic course of injury; the initial impact to the brain is referred to as the primary injury and encompasses the mechanical damage that occurs to the neurons, axons, glia, and blood vessels as a result of immediate shearing or tearing of the physical structures within the brain. Thus, the primary injury leads to hemorrhaging, contusions, immediate cell death, and dysregulation of the Blood-Brain Barrier (BBB) [6], [9]. Over time, the secondary injury occurs from minutes to months to years after the primary injury resulting from multiple, parallel cascades of biological reactions. Suspected secondary injury mechanisms include a wide variety of processes such as depolarization, disturbances of ionic homeostasis, mitochondrial dysfunction, and initiation of inflammatory and immune functions, among others [10]. These secondary injury cascades are thought to account for the development of many of the neurological deficits

observed after TBI as they result in an endless sea of damage to nervous tissue. This damage is perpetuated by the failure of neuronal energy, glial injury and dysfunction, and inflammation caused by microglia invasion into the site of injury, where they release proinflammatory cytokines [11].

Microglia cells are the primary innate immune cell in the central nervous system (CNS), and they play an active role in the brain environment after a TBI occurs [12]. Microglia can migrate to the site of injury to establish a protective environment that helps prevent any further damage from occurring. In the aftermath of a TBI, the critical function of microglial to eradicate cellular and molecular debris [11]. This process is generally seen as beneficial to have microglia present at the injury site after TBIs occur. However, if microglia activation becomes chronic, they can potentiate an inflammatory response that becomes harmful to the surrounding microenvironment [13]. Microglial activation occurs early after TBI impact and has been documented at detectable levels years after the initial injury both in vivo and post-mortem [13]. Chronic inflammation can occur because, aside from removing debris from the injury site, microglia are also capable of releasing noxious substances such as proinflammatory cytokines, reactive oxygen species (ROS) and, nitrogen species [11], [12], [14]. Depending on the surrounding stimuli in their local microenvironment, microglia can be polarized into having distinct molecular phenotypes, gene expression, and effector functions. Microglia morphology can switch from a "normal" ramified shape to a hypertrophic, "bushy" morphology depending on the proinflammatory cytokine that activates the microglia [11]. For example, proinflammatory cytokine interferon-y (IFNy) has been shown to promote a 'classical' M1 phenotype, which produces high levels of proinflammatory cytokines and

oxidative metabolites that are essential for host defense. However, these cytokines can also cause damage to healthy cells and tissue [12]. Alternatively, activating microglial cells in the presence of anti-inflammatory cytokines such as interleukin-4 (IL-4) promotes the 'alternative' M2 phenotype to be expressed [15]. In general, the proinflammatory M1 phenotype favors the production and release of cytokines that can exacerbate the neural injury.

On the other hand, the M2 phenotype is associated with the release of neurotrophic factors that promote repair and play a phagocytic role [11]. Under normal conditions, microglia possess an M2 phenotype in an intact CNS; however, after an acute TBI, it is hypothesized that M1 and M2 microglia exist in a state of dynamic equilibrium within the lesion microenvironment [15]. Thus, determining whether the microglia cells differentiate into M1 phenotypes that exacerbate the tissue injury or M2 phenotype that promotes CNS repair depends on the local signals within the region microenvironment.

1.2.2 Treatment and standard of care

Current TBI treatments are merely palliative and include life-sustaining interventions in severe cases, but few treatment options are available for more mild cases [16]. Prevailing diagnosis methods for TBI include using the Glasgow Coma Scale(GCS) to determine the severity of the injury within 48 hours of the injury [16]. GCS is currently the most common scoring system used to describe the level of consciousness in a person following a TBI [17]. Another option for assessing the damage present after a TBI occurs is with CT or MRI scans. Using neuropathological tests with computer-assisted brain scans can help health care professionals visualize brain damage that would otherwise be

missed if only relying on the GCS for diagnosis [8]. MRIs and CT scans can detect fractures, hemorrhages, swelling, and certain types of tissue damage.

It should be noted that these imaging tests are most effective at diagnosing severe cases of TBI as mild TBI often involves subtle trauma to the brain that causes chemical and physical changes to the brain tissues rather than structural damage [18]. Current treatment options for severe TBI injuries include surgery to repair skull fractures or remove hematomas and rehabilitation when the injury has left them significantly impaired [16]. Corrective surgery within four h of clinic admittance has demonstrated shorter hospital stays and a 50% lower mortality rate in TBI patients [16], [19]. These patients may also be given medications such as anti-seizure drugs or diuretics to help limit secondary damage to the brain immediately after injury [20]. It is essential to know that these medications do not help treat the damage that has already occurred but only hope to prevent further damage from happening due to potential swelling or loss of oxygen to the brain after the initial injury. For more mild cases of TBI, often there is little medical care that can be provided. A person afflicted with mild TBI will be prescribed to maintain relative resting practices for a few days, but there are currently no treatments for mild TBI [19]. The standard of care focuses on interventions that manage the symptoms caused by TBI rather than treating the root cause of the injury, such as inflammation. These interventions at acute time points are necessary to sustain life and mitigate tissue death in the brain. However, there is a need for new therapeutics that halt or ameliorate the pathophysiology of the secondary injury in the remaining viable brain tissue to improve the long-term disease management of acute brain injuries [21].

1.2.3 Drug Therapeutic options

Despite the unmet clinical need, there are currently no therapeutic treatments approved by the Food and Drug Administration (FDA) to help minimize the long-term effects of TBI [6]. Furthermore, 30 years of TBI clinical trials have not developed a single therapeutic that supports patient brain health. Although this is not due to a lack of trying, more than 30 clinical trials have investigated various compounds to treat acute TBI. Yet, no treatment has succeeded at the confirmatory trial stage [22]. A notable example of this is progesterone. Progesterone is a neurosteroid whose receptors are expressed in the CNS [23]. Neuroprotective effects for progesterone have been reported in experimental spinal cord injury (SCI), stroke and TBI. Due to promising preclinical data and positive trends seen in phase II clinical studies, two phases III multi-center clinical trials were developed [24]. Unfortunately, t phase III clinical trials ultimately concluded that progesterone did not benefit over a placebo in improving outcomes in patients with acute TBI [24]. Thus, progesterone joins the growing list of negative or inconclusive trials in the arduous search for TBI treatment despite extensive preclinical data and promising single-center trials.

This high failure rate is primarily due to TBI's many factors that translate promising agents from laboratory to clinical challenging. These factors include the heterogeneity of TBI pathophysiology, differences between animal models and the human disease, poor pharmacokinetic profiles of TBI drugs, poor drug penetration into the brain or low bioavailability of the drug, and cell-specific pharmacology [6]. The complexity and diversity of secondary injury mechanisms have led to the approach to target multiple injury factors by using multipotent drugs that can modulate numerous injury mechanisms [25]. The multi-drug approach has long been successfully employed

to treat cancer and infectious diseases. Still, it is less likely to gain traction for neuroprotection because of the costs associated with establishing even a single agent [26]. With this consideration in mind, there has been a recent emphasis on multipotent treatments[6], [18].In addition, increasing evidence in the literature underscores the importance of viewing injury more broadly to include endothelial cells, astroglia, microglia, and precursor cells [27]. More recent neuroprotection approaches have recognized this complex structure and interplay, emphasizing therapeutic strategies that promote the recovery and optimal functioning of non-neuronal cells in addition to more directly inhibiting mechanisms of neuronal cell death [25], [27].

There is considerable literature on NAC as a neuroprotective agent in preclinical models of central and peripheral nervous system injury[28]. NAC has been shown to have antioxidant and neurovascular-protective effects after preclinical TBI [29]. In addition, NAC treatment following controlled cortical impact (CCI) increased levels of anti-inflammatory M2 microglia in white matter tracts [30]. Specifically, a single dose of NAC is neuroprotective, ameliorating biochemical and histological endpoints in a rat weight drop model. Multiple doses effectively reduce inflammatory sequelae in an open skull dural impact rat model [28]. NAC's antioxidant and anti-inflammatory effects may be downstream consequences of inhibition of NAC-induced nuclear factor-kB–activated pathways that include cytokine cascades and phospholipid metabolism [31]. This pathway may also underlie the broader efficacy of NAC in rodent ischemia-reperfusion cerebral stroke models, a rodent sensory nerve axotomy model, and prevention of mitochondrial damage with loss of dendritic spines in hippocampal neurons [32].

The up-regulation of glutathione levels in the brain by systemic administration of NAC represents another potential neuroprotective mechanism. NAC is a precursor for GSH, a tripeptide derived by linking the amine group of cysteine to glycine and the carboxyl group of the glutamate side-chain [28]. GSH is a critical intracellular antioxidant that prevents damage caused by reactive oxygen and nitrogen species (ROS and RNS) [33]. GSH is generated within its target cells from the amino acids L-cysteine, L-glutamic acid, and glycine. Notably, the sulfhydryl (thiol) group (SH) of cysteine acts as a proton donor in this role and is responsible for the antioxidant activity of GSH. Moreover, this cysteine represents the rate-limiting factor in cellular GSH production since cysteine is relatively scarce, except in specific foods [33], [34].

There have also been evaluations of NAC as a countermeasure for the neurosensory sequelae of mTBI in military personnel [21]. The rationale underpinning this approach is based on the fact that NAC's mechanism of action can alleviate or prevent the cascade of pathological events seen after mTBI [35]. In addition, NAC is the active ingredient in the brand name medication Mucomyst, a compound with a thirty-year safety history in US hospitals, used for cystic fibrosis, acetaminophen poisoning, and high dye load x-rays as both an oral and an intravenous treatment [28]. As such, NAC is a "proven" medication that is a good candidate for TBI treatment as it is tolerability/safety is well characterized, as opposed to introducing previously non-utilized or non-FDA approved pharmaceuticals [35]. Historically, this has represented a more rapid and successful translational strategy than developing new previously untested drug candidates. Notably, scientists have demonstrated NAC to be efficacious in reducing the sequela of mTBI in a randomized, double-blind, placebo-controlled study examining

mTBI after blast injury [21]. Logistic regression on the outcome of 'no day seven symptoms' indicated that NAC treatment was significantly better than placebo (OR=3.6, p=0.006). Secondary analysis revealed subjects receiving NAC within 24 h of the blast had an 86% chance of symptom resolution with no reported side effects versus 42% for those seen early who received placebo [21]. This study demonstrates that NAC, a safe pharmaceutical countermeasure, has a beneficial impact on the severity and resolution of symptoms of blast-induced mTBI.

Although NAC can cross the BBB, its potential neurotherapeutic effects have mainly been limited by multiple factors. NAC has a low oral bioavailability estimated at 6-10% due to extensive first-pass metabolism [32]. In addition, when administered intravenously, NAC binds to plasma proteins, and about 30% undergoes renal elimination resulting in a short half-life. In addition, increasing systemic doses of NAC for superior (passive) transport of NAC across the BBB may increase the patient's blood pressure [28]. Incorporating NAC in a biocompatible substrate will enable localized delivery of NAC at the target site, bypassing its limitations from alternate administration routes (oral, intravenous) and thereby enhancing its therapeutic effect.

1.2.4 Using nanoparticles to treat TBI

The lack of clinical successes for TBI highlights the need to innovate in therapeutic development for brain injuries. Nanomedicines, materials with dimensions on the nanometer length scale, have been actively developed to treat cancer over the past two decades. These treatments have yielded benefits such as decreasing off-target toxicity, improving drug distribution, and incorporating challenging cargoes such as small hydrophobic molecules and labile macromolecules [26], [36], [37]. In addition,

there is a substantial body of literature that establishes a broad understanding of how the physicochemical and molecular properties of NPs affect their behavior in tumor tissues [37]. For example, the enhanced permeability and retention (EPR) effect in tumors is when NPs enter the tumor interstitial space and are retained due to compromised lymphatic filtration [26]. This effect can be optimally exploited for passive NP targeting with NPs with a hydrodynamic size of about 30 nm, while sizes between 10-100 nm still provide passible targeting [38].

Additionally, alterations in surface charge and chemistry are known to play significant roles in NP behavior within the tumor [39]. Although there are differences between TBI and cancer in disease initiation and major disease hallmarks, there are many shared disease pathologies. These disease pathologies include dysregulation of the vasculature, increased access to cells and extracellular matrix, changes in the biochemistry of the interstitial fluid, and an activated immune system. In both diseases, pathology causes vascular damage that triggers a host response such as clotting or receptor expression, which can be targeted by nanomaterials [40].

Nanoparticles (NP) are defined for pharmaceutical purposes as solid colloidal particles ranging from 1 and 1000 nm in size. They are uniquely suited to circumvent the formidable biological barriers that prevent the transport and uptake of therapies into the brain [41]. Thus, encapsulation of therapeutics within NPs is one of the approaches that can improve site-specific delivery, bioavailability, and shelf-life and circumvent any potentially deleterious effects of the delivered therapeutics. Their small size and mobility enable NPs to access a wide range of tissues and cells for extracellular and intracellular delivery [37]. The administration of NPs through microcirculation is a viable approach

for facilitating drug delivery to the brain since the diameter of the smallest capillaries is approximately 5-6 μm [36], [39]. Nps can be used to deliver various cargos, such as hydrophilic/hydrophobic drugs, proteins, vaccines, biological macromolecules, and genes [36].

For an Np delivery system to achieve the desired benefits, the residence time in the bloodstream must be long enough for the NP to reach or recognize its site of action. However, the major obstacle to realizing this goal is NP clearance from the bloodstream, where previous studies report only 1.5% of injected NPs may reach their intended target site [42]. The main NP clearance mechanisms are the same as the body's removal of foreign material from the bloodstream. These mechanisms include opsonization, renal clearance, and sequestration in the reticuloendothelial system [26], [40]. Phagocytic recognition and clearance are dependent on initial particle opsonization. However, key Np parameters have been identified to help evade clearance mechanisms, including surface modification, size, charge, and shape.

The upper size limit of NPs size is about 5-8 μm dictated by the smallest diameter of lung micro-capillaries for systemic delivery. Larger particles carry the risk of clogging the vessels. Generally, for brain delivery, NPs ranging from 100-200 nm are used for leveraging in minimal clearance NPs[43]. Studies have shown a clear inverse correlation between NP size and BBB penetration. To this end, for systemic brain delivery, the NP size plays a vital role in enabling prolonged blood circulation and access to the brain [39]. Another critical consideration when designing NP for systemic delivery is the surface charge, which influences clearance and stability in circulation. Here one must consider the impact blood proteins and cells have on the stability of NPs in vivo. Generally,

negative NPs (-40 mV) exhibit strong MPS uptake, and positive NPs (+40 mV) induce serum protein aggregation. Nps with neutral charge (within +/- 10mV) exhibit the least RES interaction and the longest circulation in vivo [41].

The morphology and shape of the NPs also contribute significantly to cellular uptake, transport, and biodistribution. Round shape/spherical NPs are the most common due to their ease of synthesis and fast rate of endocytosis. In contrast, other shapes like rods or disks have gained attention for their advantage in cellular internalization and drug loading efficiency [36]. For example, shape-induced NP enhancement of vascular targeting in the brain via receptor-mediated delivery was confirmed by Kollhar. Furthermore, the rod-shaped polystyrene NPs decorated with an anti-transferrin receptor antibody showed a 7-fold increase in brain accumulation compared to NPs with spherical shapes with the same surface chemistry [41]. Taken together, systemically delivered NPs eventually clear from the bloodstream through renal clearance, phagocytosis, or RES interaction [44]. The parameters outlined above describe strategies to slow this process by escaping different clearance mechanisms leading to prolonged blood circulation and increased delivery to the brain.

Passive delivery of NPs in the brain predominately relies on the functional state of the BBB. Particular pathological events such as inflammation or hypoxia have previously been shown to disrupt the usually tightly regulated BBB to produce leaky blood vessels [45]. These permeable blood vessels provide an opportunity for the systemically circulating NPs to extravagate and spontaneously accumulate in the brain's interstitial space. Analogous to the EPR effect seen in tumors, a dysfunctional BBB occurs after brain injury, leading to the opening of the tight junctions resulting in a leaky vasculature

[38]. This event allows the Nps to accumulate in the brain parenchyma due to increased paracellular permeability. However, the BBB permeability is transient, and the NP delivery timing needs to be fine-tuned to take advantage of these changes in the membrane permeability [46].

Although passive delivery may facilitate the transport of NPs through BBB, poor distribution of NPs in the brain remains a challenge. This active transport has been commonly explored to enhance selective targeting and reach the intercellular compartment after delivery [43]. Active transport relies on energy-dependent cellular processes to bind to a target cell surface receptor, be internalized into the target cells, and then transported either to an intracellular site of action or transcellular into the injured brain parenchyma [26], [36], [41]. In addition, retention of passively targeted NPs within the injured brain may be enhanced by a more active delivery approach by attaching targeting moieties such as peptides or antibodies to the surface of the NP [38], [45].

1.2.5 Nanoparticle composition

Nanoparticles can be synthesized using various materials and protocols where the parameters are trailered to design the desired NPs. The essential characteristics for drug delivery considerations are size, payload encapsulation efficiency, and payload release characteristics [36]. The ideal properties of NPs for brain drug delivery are not only to be non-toxic, biodegradable, and biocompatible but also to have physical stability in blood with prolonged blood circulation and the ability to cross BBB [47]. Different NPs used for brain injury applications include polymeric Nps, lipid Nps, inorganic Nps, and hybrid Nps [48].

Polymeric NPs made up of a polymeric core or shell can be formulated to potentially penetrate the BBB, encapsulate various drug formulations, and facilitate targeted delivery[47]. Thus, it is not surprising that polymeric NPs are the most popular Nano-platforms for neurological diseases. The most common preparation methods include solvent evaporation, polymerization methods, and solvent diffusion, such as single- and double-emulsion methods [44]. In addition, polymeric Nps can be used for the controlled release of bioactive agents and improve drug solubility, stability with enhanced efficacy, and reduced toxicity [49].

Among the synthetic polymers, poly (lactic-co-glycolic acid) PLGA (obtained by the condensation of lactic acid and glycolic acid) is considered a base material for numerous biomedical applications. The main appeal of PLGA NPs is that they are hydrolyzed into their monomeric units, such as lactic acid and glycolic acid, which are byproducts of various metabolic pathways in the body under normal physiological conditions [41], [50]. Technological sophistication has enabled PLGA nanoparticles to be explored to encapsulate anticancer drugs, diabetic medications, or hormones and offer a platform for multifunctional imaging in cancer diagnostics [51]. One of the lures of using PLGA in medical devices or nanoparticle fabrication is that the rate of biodegradation can be controlled by adjusting its molecular weight (MW) or copolymer ratio [52]. In addition, the US FDA and the European Medicine Agency EMA have permitted the use of PLGA for drug delivery applications in humans [36].

The application of PLGA as a biomaterial dates back to the 1970s when it was developed as a material for biodegradable sutures, followed by its use in devices such as implants, tissue grafts, prosthetic devices, and therapeutic devices [37], [50]. Now the

technology has matured to the nanoscale. PLGA has been used to encapsulate various types of drugs, such as paclitaxel, doxorubicin, cisplatin, docetaxel, and curcumin [26], [51]. In addition, PLGA particles offer several advantages for biomedical applications: they can be targeted in vivo using antibodies, protect DNA and other biomolecules from degradation, or effectively enhance immune response when modified with targeting ligands [41]. Finally, aiming at clinical use, they can be stored for lengthy periods in a powdered form [50]. Currently approved PLGA particles include Lupron Depot (Abbott Laboratories, USA) and Trelstar (Watson Pharmaceuticals, USA), which are used for sustained release of leuprolide and triptorelin, respectively [43], [53]. Additionally, several ongoing and recently completed clinical trials involve using PLGA as bioscaffolds, biodegradable polymer stents,r bioabsorbable screws[36].

The properties of PLGA particles are strongly dependent on the preparation method. Specific applications, e.g., cell targeting, imaging, and therapeutic delivery, require particles with well-defined physicochemical properties [37]. PLGA is a linear copolymer with lactic and glycolic acid repeat units, organized as a block-co-polymer or statistical polymer [43]. The body can efficiently metabolize both monomers into carbon dioxide and water via the tricarboxylic acid cycle, resulting in minimal systemic toxicity. PLGA can be synthesized by direct polycondensation of lactic and glycolic acid, resulting in copolymers with low molecular weight and broad molar mass distribution [54]. The ring-opening polymerization of cyclic dimers can obtain polymers with higher molecular weight and narrower molar mass distribution. In general, the molecular weight of PLGA can be adjusted from 4 to 240 kDa by changing the polymerization conditions and the ratio of monomer to initiator [54]. The biodegradation rate of PLGA depends on

several factors, e.g., the composition of the polymer and its microstructure. The degradation of PLGA is faster for polymers with the increased amount of glycolic acid units [41]. Polymers with a 50:50 ratio of lactic and glycolic acids have the most rapid degradation rate and are therefore one of the most frequently used polymers in nanomedicine. PLGA with the 50:50 ratio has a degradation rate of around two months in vivo and has the fastest release rate compared to other ratios [47]. PLGA can be dissolved in a range of common organic solvents, depending on its composition. PLGA with a higher amount of lactic acid is dissolved by chlorinated solvents, such as dichloromethane or chloroform, and water-miscible solvents, like acetone or tetrahydrofuran. PLGA with a higher amount of glycolic acid is dissolved by fluorinated solvents, like hexafluoroisopropanol [55]. The physicochemical properties of PLGA particles primarily depend on the properties of PLGA polymer used for synthesis, including the ratio of lactic acid to glycolic acid, molecular weight, and storage temperature [53]. However, most of the particle properties, for example, particle size and size distribution, are strongly dependent on the synthesis method in general and influenced by the synthesis parameters within the same method in particular, including the addition of encapsulated substance [44]. PLGA particles can be functionalized with polyethylene glycol (PEG) or other hydrophilic polymers resulting in particles with a "stealth" surface [42]. These stealth particles become almost invisible to the reticuloendothelial system, responsible for the clearance of particles from the bloodstream, and have prolonged circulation.

Furthermore, coating materials may improve the production of particles with well-controlled and reproducible sustained-release profiles [56]. PEG is a water-soluble,

non-ionic polymer, which has become a gold standard for the stealth modification of nanoparticles to increase their blood circulation time [36]. PEG has good synthesis flexibility, and its end groups can be easily modified. The addition of PEG layer can enhance particle hydrophilicity, resulting in reduced interactions with biomolecules, e.g., lipids or serum proteins, and therefore protect particles from elimination from the bloodstream through the RES [57]

For this study, I work on synthetic PLGA polymer and PEG to create a biocompatible nanoparticle capable of encapsulating drug therapeutics.

1.3 Aims

The main objective of this thesis was to generate and characterize a reproducible PEG-PLGA nanoparticle platform that reduces RES clearance in vivo and shows sustained drug release over time for an encapsulated model hydrophobic dye. In addition, the encapsulation ability of the hydrophilic TBI drug candidate NAC with the generated PEG-PLGA synthesis protocol was also determined. This main objective was broken down into three achievable sub aims, which are as follows:

- Synthesize PEG-PLGA nanoparticles with a reproducible diameter of 200nm and determine particles encapsulation efficiency and drug loading capacity
- Achieve degradation and drug release from PEG-PLGA nanoparticle in situ over two weeks and determine drug release in vitro
- Determine if PEGylating nanoparticles results in increased passive targeting of PEG-PLGA nanoparticles into the injured brain in an animal model of TBI

Materials & Methods

2.1 Materials & Methods

2.1.1 Single emulsion-solvent evaporation synthesis of PLGA nanoparticles

Nanoparticles loaded with DiI or DiO were synthesized by a single-emulsion solvent evaporation technique. Fifty milligrams of PLGA (50:50, Ester terminated) and 25uL of 10mg/mL dye in DMSO were dissolved in 1 mL DCM. The polymer/drug solution was then added dropwise to 2 mL of 2% polyvinyl alcohol (PVA) as the outer aqueous phase and sonicated to form an emulsion. Particles were ultrasonicated for 10 seconds 9 times with 30 seconds of rest on ice between each round. Sonicator was set to 30% amplitude using a 1/8 in probe tip size. The emulsion was poured into a beaker containing aqueous 2% (vol/vol) PVA and stirred at room temperature overnight to allow the solvent to evaporate and particles to harden.

Following the solvent evaporation phase, the nanoparticle solution was subjected to typical centrifugation speeds (17,000 × *g* for 15 min, three times), and the pellet was collected. Washed particles were suspended in a 5% sucrose solution immediately before lyophilization.

2.1.2 Double emulsion-solvent evaporation synthesis of NAC encapsulated PLGA nanoparticles

Nanoparticles loaded with NAC were synthesized by a double-emulsion solvent evaporation technique. First, a 100mg/mL NAC solution was made, 100uL of NAC solution was then added dropwise to fifty milligrams of PLGA dissolved in 1 mL of DCM. The solution was then ultrasonicated for 10 seconds 9 times with 30 seconds of rest on ice between each sonication. The First emulsion was then added to 2 mL of 2% PVA dropwise while vortexing. The Ultrasonication process from above was repeated to form a double emulsion. The emulsion

was poured into a beaker containing 2% PVA and stirred at room temperature overnight to allow the solvent to evaporate and particles to harden. The nanoparticle solution was then subjected to typical centrifugation speeds (17,000 x g for 15 min, three times) in DI water to was the particles. The pellet was collected and re-suspended in a 5% sucrose solution immediately before lyophilizing to prevent nanoparticle aggregation. Doped NAC particles were made in the same way but had NAC added to the aqueous PVA solutions so that it was a 2.5% NAC concentration w/vol [44].

2.1.3 PLGA particle size

The size distribution of nanoparticles was measured via dynamic light scattering (DLS). Briefly, one μL of the 10 mg/mL particle suspension was diluted to 49 μL of 1x PBS to avoid multiple scattering events. The measurements were obtained at room temperature (25 °C ± one °C), at which the corresponding water viscosity and refractive index were 0.872 and 1.330 cP, respectively. An average of three measurements was used to report the Z-average values for each sample.

2.1.4 Encapsulation Efficiency and Loading capacity of PLGA nanoparticles

The EE and DL of PLGA NP were determined by a UV–visible spectrophotometer. One milligram lyophilized PLGA NP was accurately weighed, and DiI in PLGA NP was extracted by adding 1 ml dichloromethane. The above extract was measured at the wavenumber of 478 nm. The EE and LC were calculated using the following equation:

$$\text{Encapsulation efficiency} = \frac{\text{Total drug amount} - \text{Free drug amount}}{\text{Total drug amount}} \times 100$$

$$\text{Loading efficiency} = \frac{\text{Encapsulated drug amount}}{\text{Nanoparticle weight}} \times 100$$

2.1.5 Stability Assessment of PLGA Nanoparticles in Situ

PLGA nanoparticles encapsulating D and A dyes (referred to as "FRET NP") were studied in situ to determine dye release and particle integrity. A suspension of FRET NP in deionized water was incubated at 37 °C for three weeks. Emission spectra were measured at different time points. In addition, PLGA nanoparticles encapsulating the only donor DiO green dye and acceptor DiI dye were studied in parallel as a control. The recovery of FRET-quenched D emission was monitored using fluorescence spectroscopy and was compared to variations of the DiO NP emission; thus, the influence of direct DiI excitation was excluded from the analysis. This process was repeated for nanoparticles incubated in PBS buffers at pH 7.4 and pH 5.8 for three weeks [58].

2.1.6 Cell Culture

BV2 microglia were placed in MEM/EBSS medium containing 10% fetal bovine serum (FBS) and 100 U/ml penicillin and streptomycin and cultured at 37◦C in an incubator at 95% O2/5% CO2 atmosphere. Every 2–3 days, the cells were washed twice with phosphate-buffered solution (PBS). After using a cell scraper to dislocate attached cells, the cells were transferred into a new flask containing MEM/EBSS medium (supplemented with 10% FBS and 100 U/ml penicillin and streptomycin) placed in the incubator. When cells grew adherent and the cell body is branched, they were transferred into 24-well plates (80 cells/well for immunofluorescence) or 96-well plates (40 cells/well for cell viability assay).

2.1.7 Stability Assessment of PLGA NP in Vitro

BV-2 cells were grown for 48 h at 50% confluency on cover glasses coated with 10ug/mL poly-D-lysine. Cells were labeled with the particles at a concentration of 1 mg of nanoparticles per million cells and were incubated for different time points (1, 24, 48, and 72 h). At each time point, the cells were fixed and prepared for fluorescent microscope imaging. FlowJo analysis software was used to determine the mean fluorescence intensity of cells [56], [58].

2.1.8 Cell Labeling and Viability

Freshly collected BV2 cells were counted (>93 % viability) and dispensed into 96-well plates at the final density of 3.0×10^4cells/100 µl/well. After a 24-h incubation to allow cell attachment, the cells without any treatment were used as control. The others were incubated with PLGA NP for 24 h with the highest concentration being 5 mg/mL. Cell viability was evaluated with an MTS assay. In brief, 20 µL of MTS was added to each well. Cell viability was determined by measuring the absorbance at 490 nm using Tecan Spark. Three replications of each sample were analyzed in each group.

2.1.9 Controlled cortical impact model

Traumatic brain injury (TBI) was modeled using the well-established controlled cortical impact (CCI) injury model56. Briefly, adult C57Bl/6 mice (8–9 weeks old) were anesthetized with isoflurane (3% induction, 1.5% maintenance) and placed in a stereotaxic frame. The

frontoparietal cortex was exposed via 3mm craniotomy, and the impact tip was centered at −2mm bregma and 1.5mm lateral from midline. The impactor tip diameter was 2mm, the impact velocity was 6.0m/s and the depth of cortical deformation was 2mm and 100ms impact duration. The skin was sutured, and the animals were placed in a 37 °C incubator until consciousness was regained.

2.1.10 Biodistribution of PEGylated PLGA Nanoparticles

BL6J mice (male, 8-9 wk old) were systemically (tail-vein) injected with PEGylated PLGA NPs. After two hours, the mice were anesthetized (isofluorane) and perfused with D-PBS (transhepatic perfusion followed by transcardial perfusion) before organs were collected into D-PBS and weighed. Organs were then submerged in 4% PFA (4 °C, 24 h), followed by cryoprotection in 20% sucrose (4 °C, 24 h). The hemisphere was then cryosectioned into 10-μm slices and mounted onto glass slides for immunostaining and imaging.

Results

3.1 Formulation and Characterization of Dye-Loaded PLGA Nanoparticles

PLGA nanoparticles (PLGA NPs) encapsulating fluorescent DiI dye were prepared via a single emulsion solvent evaporation method as shown in (**Scheme 1)**. An organic solvent (DCM) containing PLGA and DiI was mixed with a 2% PVA aqueous phase, the mixture emulsified through 90 seconds of ultrasonication. The excess organic solvent was allowed to evaporate overnight as PLGA NPs hardened. The hydrophobic nature of DiI allowed for its encapsulation within PLGA NPs during the particle formation, making DiI an adequate drug model for small molecule hydrophobic drugs. 50:50 PLGA NPs varying concentrations of PEG had an average

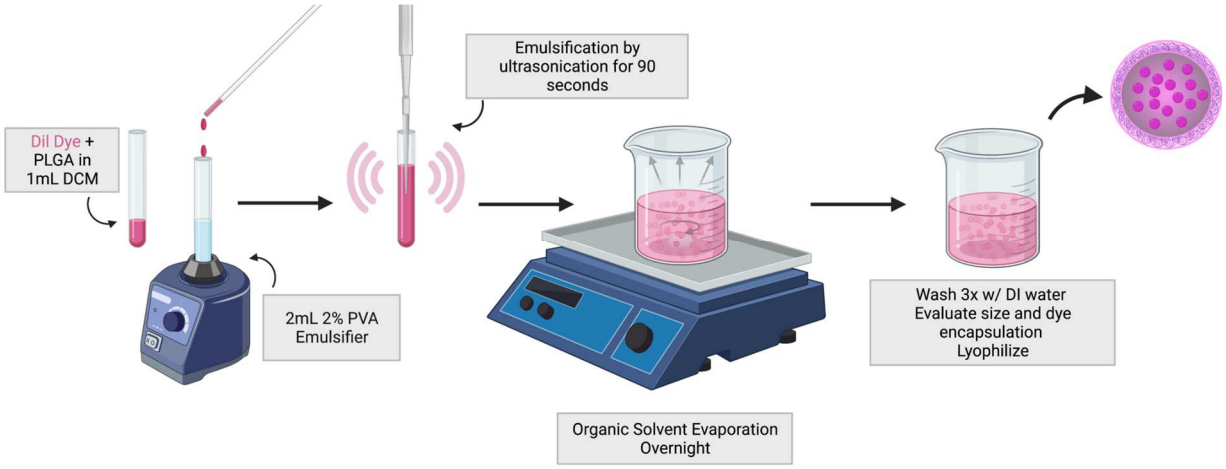

Scheme 1. Preparation of PLGA nanoparticles by the single emulsion solvent evaporation method for the encapsulation of hydrophobic cargo

Diameter of -200 nm (PDI <0.1) when synthesized using this single emulsion method (**Fig. 1a**). The NPs were characterized using dynamic light scattering (DLS) to determine the hydrodynamic diameter of the synthesized particles (**Fig. 1b**). To determine the success of the dye encapsulation after synthesis encapsulation efficiency (EE%) and loading capacity (LC%) was calculated. A DiI EE of 55%, 56%, 41%, and 36% for No, 10%, 20%, and 50% PEG respectively. LC was calculated for the dye-loaded PLGA NPs at 1.78%, 1.85%, 1.33%, and 1.16% for No, 10%, 20%, and 50% PEG loading capacity respectively (**Fig. 1c&d**).

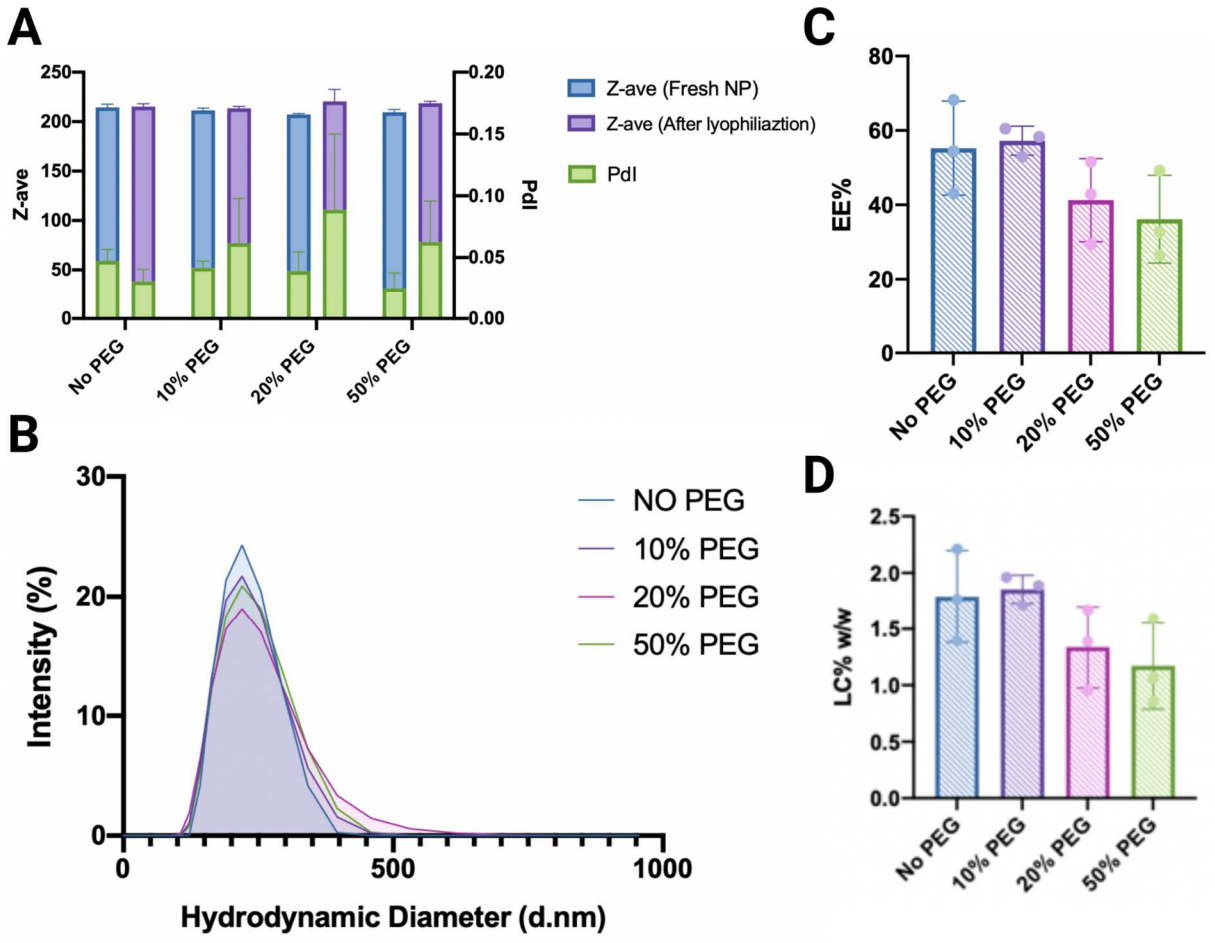

Figure 1. Characterization of varied PEG concentration PLGA nanoparticles. (A) Z-ave and polydispersity index (PdI) of PEGylated 50:50 PLGA nanoparticles, made using single-emulsion synthesis method, before and after lyophilizing. (B) Size distribution of No PEG, 10% PEG, 20% PEG, and 50% PEG-PLGA NP. (C) Encapsulation efficiency of Polyethylene Glycol (PEG) attached Ploy(Lactic-co-Glycolic Acid) (PLGA) nanoparticles (Nps). (D) Loading capacity of PEGylated PLGA NP.

3.2 Formulation and Characterization of NAC-Loaded PLGA Nanoparticles

To determine the capabilities of the developed synthesis method at encapsulating hydrophilic drugs, NAC-PLGA nanoparticles (NAC-PLGA NPs) were made. NAC-PLGA NPs were prepared via a double emulsion solvent evaporation method, as shown in (**Scheme 2)**. First, a 100mg/mL stock solution of NAC dissolved in water was prepared. The first emulsion is formed through ultrasonication by adding the NAC stock solution to PLGA dissolved in organic

solvent (DCM). The first emulsion is mixed with a 2% PVA aqueous phase; the mixture forms a double emulsion after the second round of ultrasonication. The excess organic solvent was allowed to evaporate overnight as PLGA NPs hardened. The hydrophilic nature of NAC makes it challenging to encapsulate within PLGA NPs during particle formation. Double emulsion methods are meant to aid in the encapsulation process, but EE and LC are often low when encapsulating hydrophobic drugs. To help encourage what little NAC might be encapsulated during synthesis aqueous phases of the synthesis can be doped with NAC. This helps to lessen the concentration gradient between encapsulated NAC and the aqueous environment surrounding the NPs. 50:50 PLGA NPs with an average diameter of -200 nm (PDI <0.1) were obtained using this double emulsion synthesis method (**Fig. 2a**). The PdI of the particles did increase after

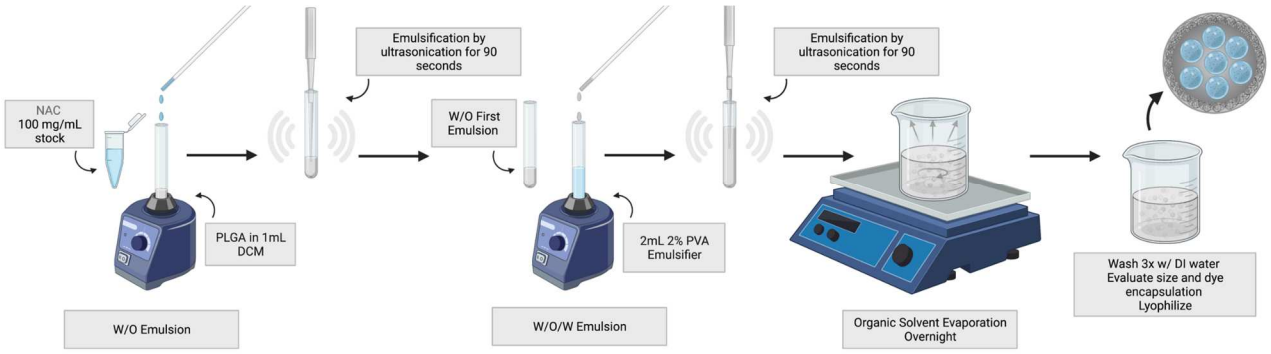

Scheme 2. Preparation of PLGA nanoparticles by the double emulsion solvent evaporation method for the encapsulation of hydrophilic cargo.

lyophilization occurred but remained under <0.1, indicating that the NPs were still monodisperse. The NPs were characterized using DLS to determine the hydrodynamic diameter of the synthesized particles (**Fig. 2b**). Doped NAC-PLGA NPs had a smaller hydrodynamic diameter (190 nm) than non-doped NAC-PLGA NPs (220 nm). EE and LC were calculated for NAC-PLGA NPs with doped and non-doped particles having 0.6% and 0.7% EE, respectively (**Fig. 2c**). LC was calculated as 0.21% and 0.19% for doped and non-doped particles, respectively (**Fig. 2d**).

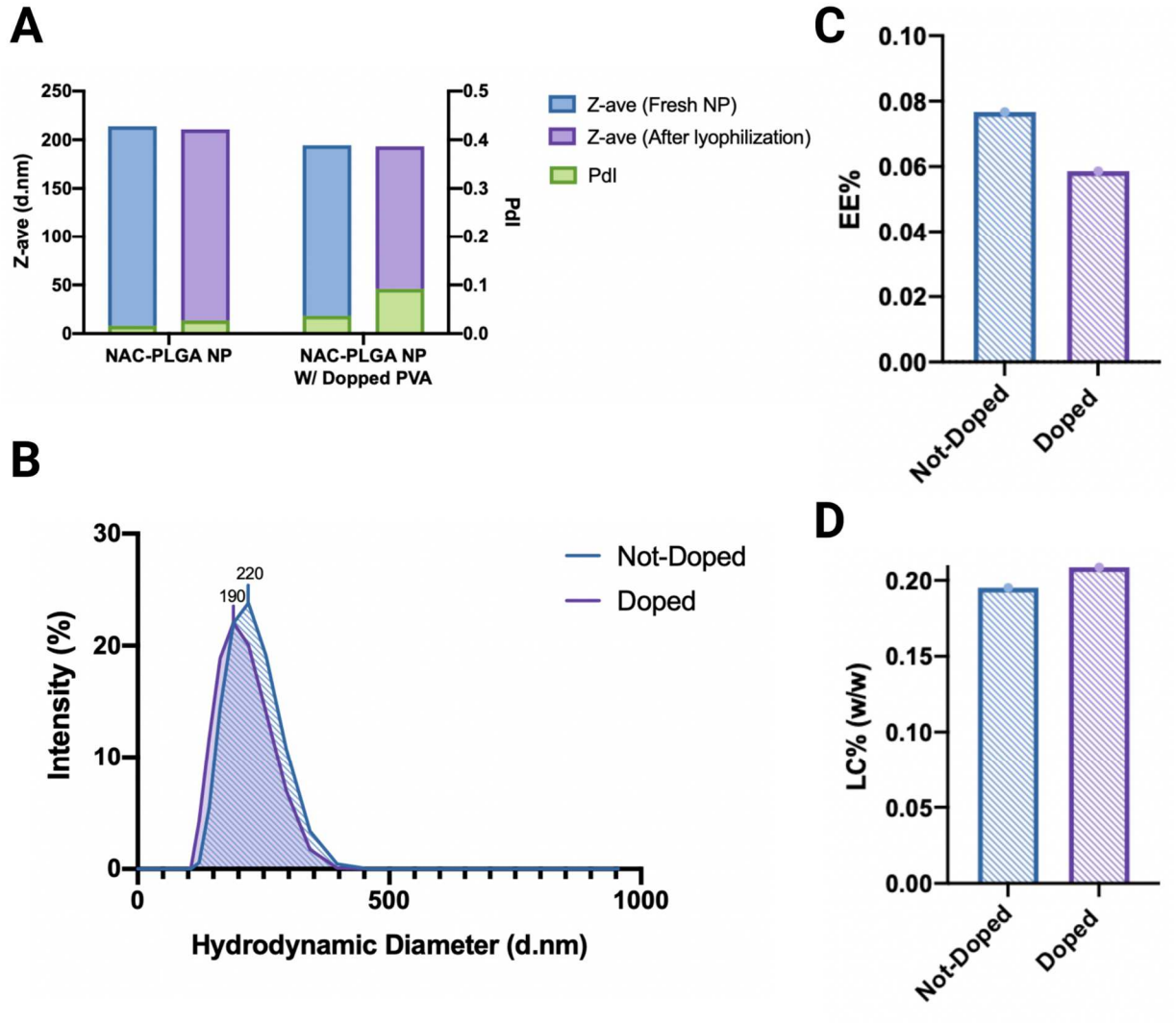

Figure 2. Characterization of NAC encapsulated PLGA nanoparticles. (A) Z-ave and polydispersity index (PdI) of N-acetyl cysteine-PLGA nanoparticles (NAC-PLGA Nps) were made using the double-emulsion synthesis method before and after lyophilizing. (B) Size distribution of freshly synthesized NAC-PLGA NP, comparing NAC doped aqueous phases during synthesis to non-doped synthesis where doped synthesis had 2.5% w/v of NAC added to PVA aqueous phases to minimize NAC concentration gradient. (C) Encapsulation efficiency of 50:50 NAC-PLGA NP. (D) Loading capacity of 50:50 NAC-PLGA NP.

3.3 Assessment of PLGA Nanoparticles Dye Release and Particle Stability in Situ

To determine the rate at which dye is released from the PLGA Nps, the optical and colloidal analysis of FRET NPs in aqueous solutions at 37C enabled the particle stability assessment in situ. DiO and DiI were selected as the donor-acceptor pair, respectively, due to their sizeable spectral overlap. PLGA NPs encapsulating only donor (DiO nanoparticles), only acceptor (DiI nanoparticles), and a combination of donor/acceptor dyes (FRET nanoparticles were prepared using the single emulsion synthesis method (**Fig. 3b**). As the dye is released from the FRET NPs, it is expected to see a loss of acceptor sensitization as the distance between the donor (D)-acceptor (A) becomes too large for efficient energy transfer (**Fig. 3a**). Fluorescence analysis revealed quenching of D emission accompanied by a sensitized A emission for FRET NPs compared to the emission spectra of DiO NPs and DiI NPs (**Fig. 3c**). Disassembly of FRET Nps upon resuspension in 50% DMSO resulted in the recovery of D emission and loss of A sensitization (**Fig. 3d**). Loss of A emission indicates the relevance of emission characteristics to the structural integrity of PLGA Nps. Relying on these observations, the spectral changes of FRET Nps were monitored under different physiological conditions to obtain information on the structural changes of NPs that result in an increase in the D-A separation distance, such as dye release.

The FRET ratio $I_R/ (I_G + I_R)$ was calculated where I_R and I_G were fluorescence intensities of DiI at 565 nm and DiO at 501 nm, respectively. The initial FRET ratio of intact NPs was measured to be 0.87, and accordingly, the FRET ratio decreased to 0.32 after particles were dissolved in DMSO. Fluorescence emission spectra of NPs were measured at different time points up to 3 weeks in deionized water, PBS PH 7.4, and PBS PH5.8. Rapid recovery of D emission was observed within the first 24 hours of incubation but then stabilized for the remainder of the three weeks. NPs in deionized water maintained the highest FRET ratio

throughout the incubation, starting at 0.87 and decreasing down to 0.80, 0.81, and 0.83 for No PEG, 10% PEG, and 20% PEG, respectively (**Fig. 4a&d**). Meanwhile, the particles incubated in PBS PH 5.8 saw the largest decrease in FRET signal with ratios decreasing to 0.69, 0.74, and 0.77 for No PEG, 10% PEG, and 20% PEG, respectively (**Fig. 4c&d**). FRET ratios for particles incubated in PBS PH 7.4 had an intermediate level of signal decrease with final ratios of 0.78, 0.78, and 0.81 for No PEG, 10% PEG, and 20% PEG, respectively (**Fig. 4b&d**).

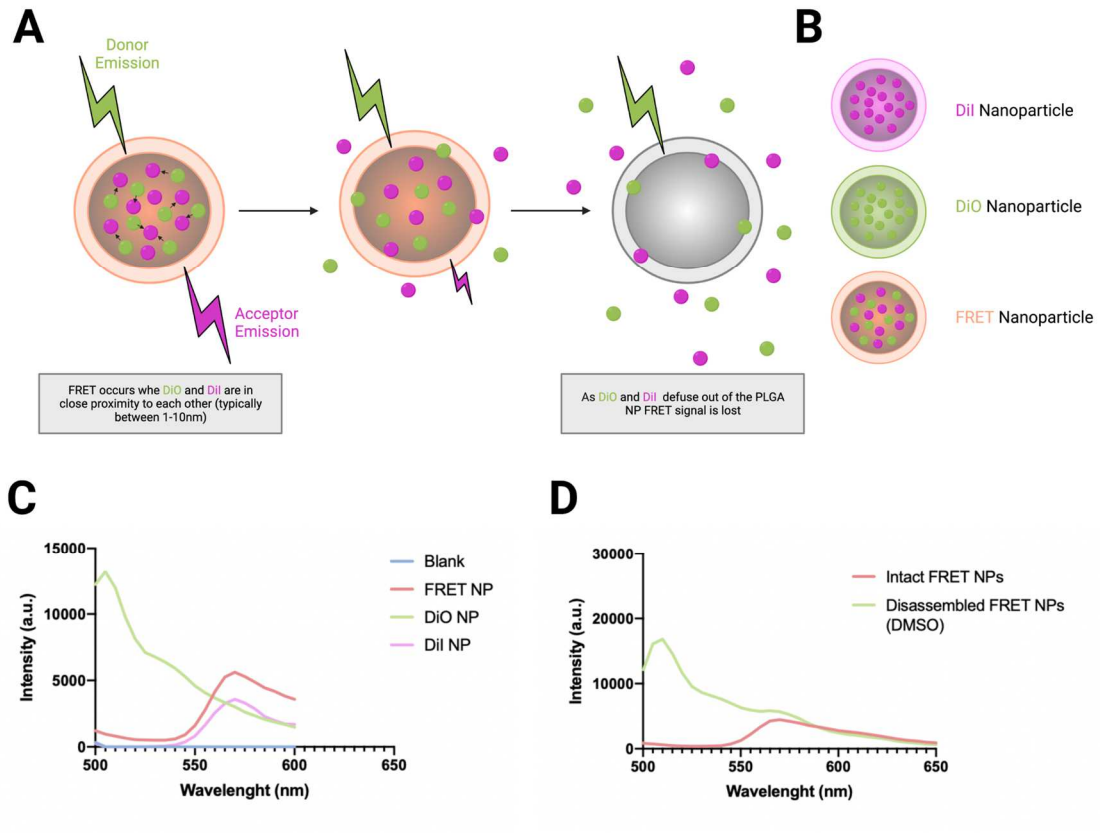

Figure 3. FRET PLGA nanoparticles feasibility of dye release characterization. (A) Schematic illustration for the dye release of DiO and DiI from FRET nanoparticles and the resulting loss of FRET excitation signal. (B) illustration of nanoparticles synthesized and used during FRET *in situ* studies. (C) Emission spectra of DiO NPs loaded with 0.25% DiO (green), DiI NPs loaded with 0.25% DiI (Pink), and FRET NPs coencapsulating 0.25% DiO and 0.25% DiI (orange). (D) Emission spectra of intact FRET NPs dispersed in water (orange) and disassembled FRET NPs dispersed in 50% DMSO (green).

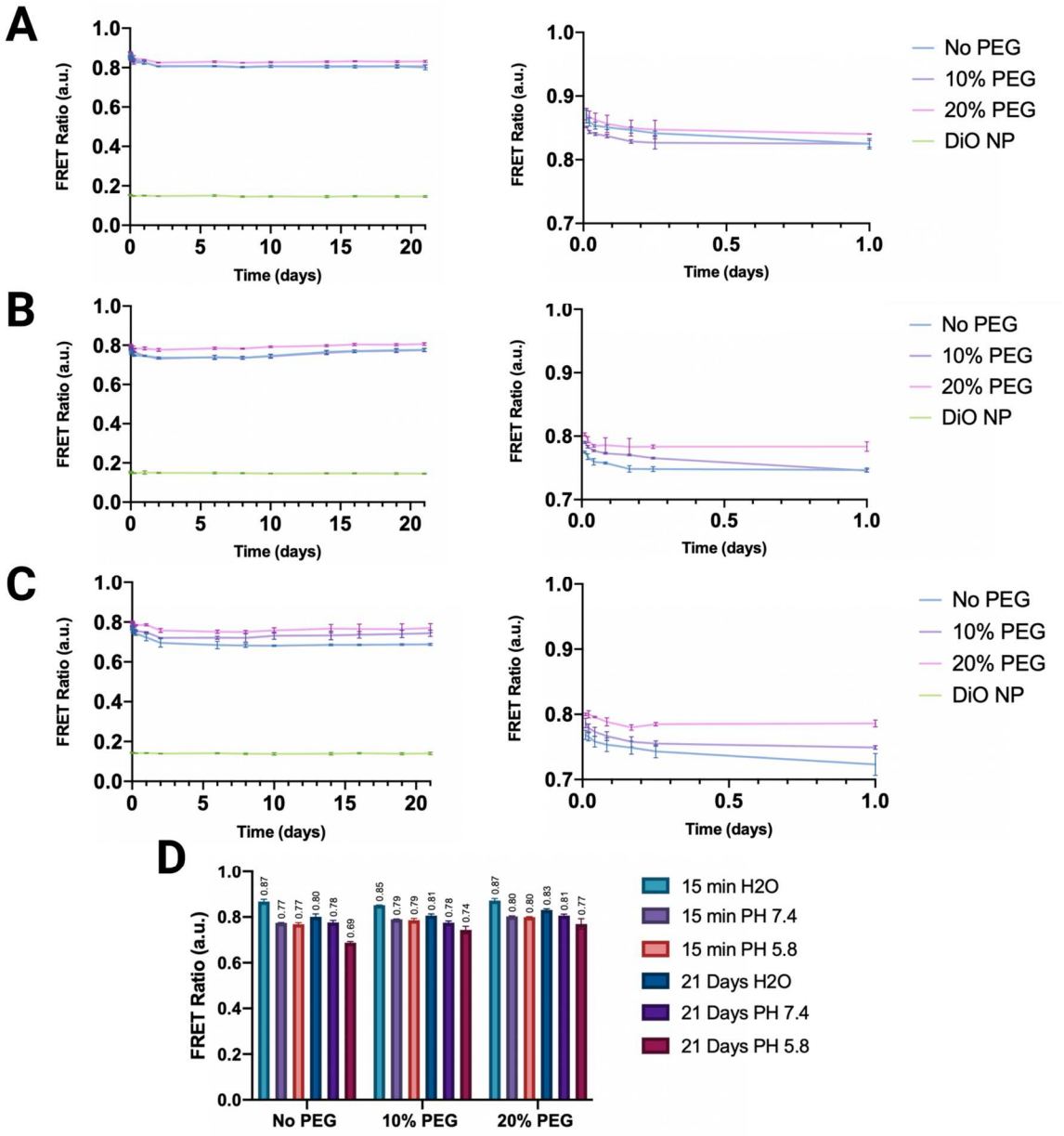

Figure 4. Stability assessment of PLGA NPs *in situ*. FRET ratio plot for FRET PEGylated NPs and DiO NPs (green) at different measurement time points dispersed in deionized water (A), PBS buffer with pH 7.4 (B), and pH 5.8 (C). The left graph shows an enlarged x and y-axis to better depict the burst-release effect seen in the first 24 hours of particle incubation. (D) FRET ratio of PEGylated NPs at 15 min and 21 Day time points.

3.4 Assessment of Cellular Uptake and Particle Stability in Vitro

In vitro particle stability assessment was performed on BV-2 Microglia cells. Cells incubated with FRET NPs and DiO NPs/ DiI NPs as controls were analyzed with fluorescence microscopy imaging at one h, 24h, 48h, and 72h after an initial 18h incubation time (**Fig. 5a**).

Fluorescence microscopy images were obtained using excitation and emission filters suitable for detecting DiO and DiI, respectively. An efficient acceptor excitation was observed at one h and 24h of incubation, as indicated by the bright yellow fluorescence intensity for FRET NPs (**Fig. 5a**). At 72h, decreased FRET fluorescence revealed that there was minimal efficient energy transfer at this time between donor and acceptor dyes, indicating that NPs have almost entirely released all encapsulated dye. Cell viability after incubation with PLGA NPs was also determined using BV-2 Microglia cells. Cells were incubated with increasing concentrations of PLGA NPs (0.004 – 5 mg/mL) for 24 hours. Cell viability was then assessed using an MTS assay (**Fig. 5b**). Cell incubated with No PEG or 10% PEG PLGA NPs saw 100% +/- 10% cell viability. While cells incubated with 20% PEG PLGA NPs had cell viabilities well over 100%, some NP concentrations reach as high as 170%.

3.5 Assessment of PEG-PLGA NPs ability to avoid RES clearance *in vivo*

To determine if synthesized PEG-PLGA NPs were suitable for in vivo studies particles were incubated in exosome-free serum for 30 min (**Fig. 6b**). The hydrodynamic diameter of the PLGA NPs remained constant after serum incubation with no presence of aggregates. The PdI of 20% PEG-PLGA NPs remained the same after serum incubation, with all other particle formulations experiencing an increase in PdI but remained well under <0.1. 50% PEG-PLGA NPs experience the greatest increase in PdI after serum incubation at 0.06. 50% PEG particles also had low EE and LC measurements. For these reasons, it was deemed that 50% PEG-PLGA NPs were not ideal for PLGA synthesis and therefore were not included in future *in vivo* studies. PLGA NPs with encapsulation efficiencies of 54%, 52%, and 51% were used for No PEG, 10% PEG, and 20% PEG, respectively, for biodistribution studies. To ensure that intact PLGA-NPs absorbance readings matched EE measurements calculated earlier, absorbance readings of

PEGylated particles were measured in triplicate (**Fig. 6c**). *in vivo* PLGA particle biodistribution was assessed using 8-9-week-old BL6J male mice. A controlled cortical impact (CCI) injure was administered at -2 left, -1.5 caudal of bregma. Two hours after injure, approximately 50mg/kg of particles were injected into each mouse, with particles being DiI concentration matched to 0% PEG particles. Two hours after injections, mice were perfused (**Fig. 6a**).

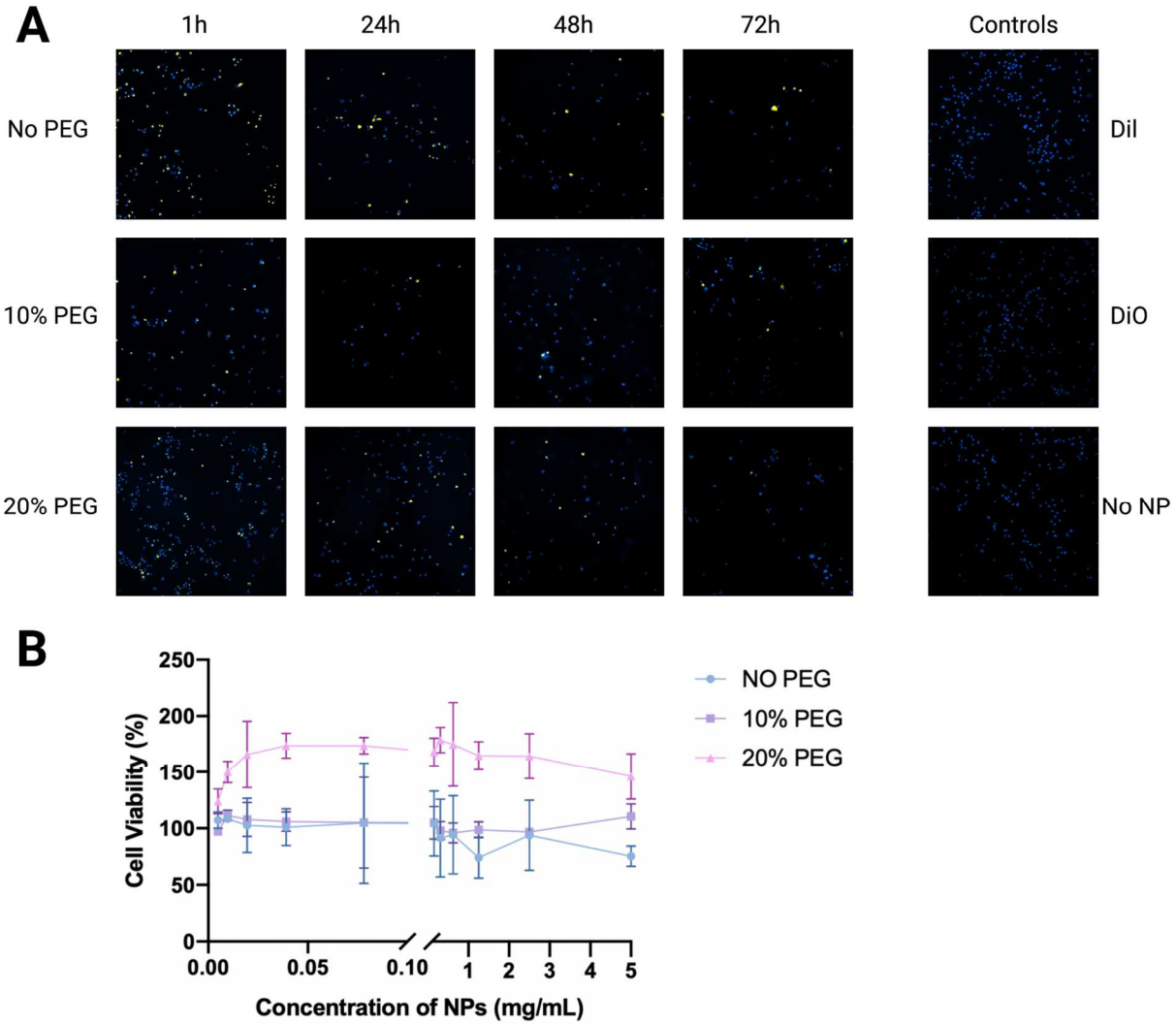

Figure 5. Stability assessment of PLGA NPs *in vitro*. (A) Fluorescence microscopy images of BV-2 microglia-like cells incubated with FRET NPs for 1, 24, 48, and 72 h collected at the red emission channel (yellow). Cell nuclei are stained with Hoechst (blue). BV-2 cells are roughly ~10 to 15 um (B) Cell viability of BV-2 microglia cells after 24 h incubation with PEGylated PLGA NPs.

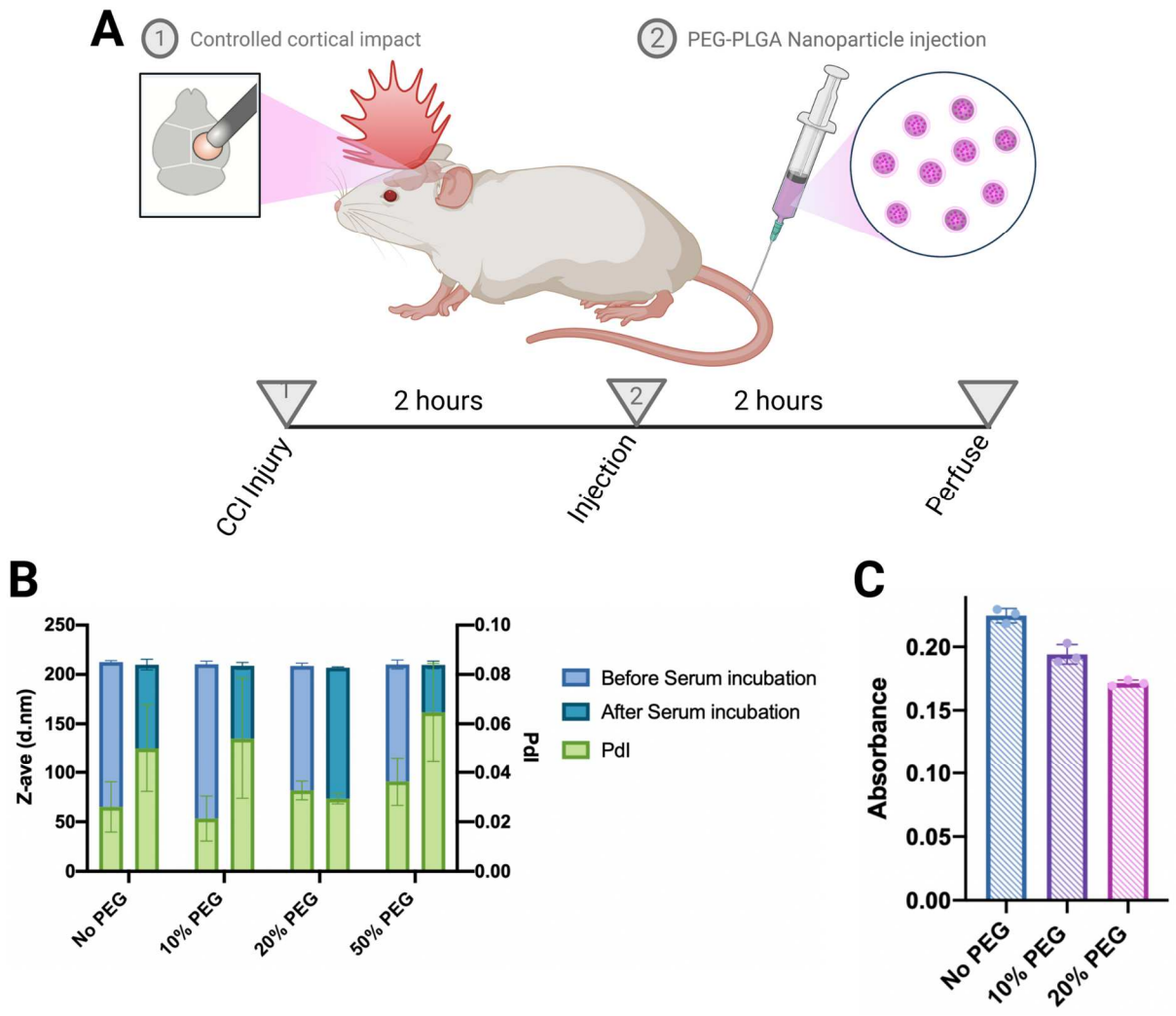

Figure 6. Experimental design of in vivo biodistribution study of PEGylated PLGA particles. (A) Overview of PEG-PLGA in vivo experimental design. (B) Serum stability test measuring particle diameter by DLS in the presence of exosome-free serum, incubated for 30 minutes. (C) Absorbance measurements of intact PEGylated particles to confirm that the absorbance readings of intact particles are similar to that for EE% measurements.

Fluorescent imaging of off-target organs shows decreased accumulation in the liver and kidney as PEG concertation on PLGA NPs increases (**Fig. 7**). There is also evidence of NP accumulation in the brain, with 20% PEG having more pronounced NP accumulation near the corpus callosum (**Fig. 8**).

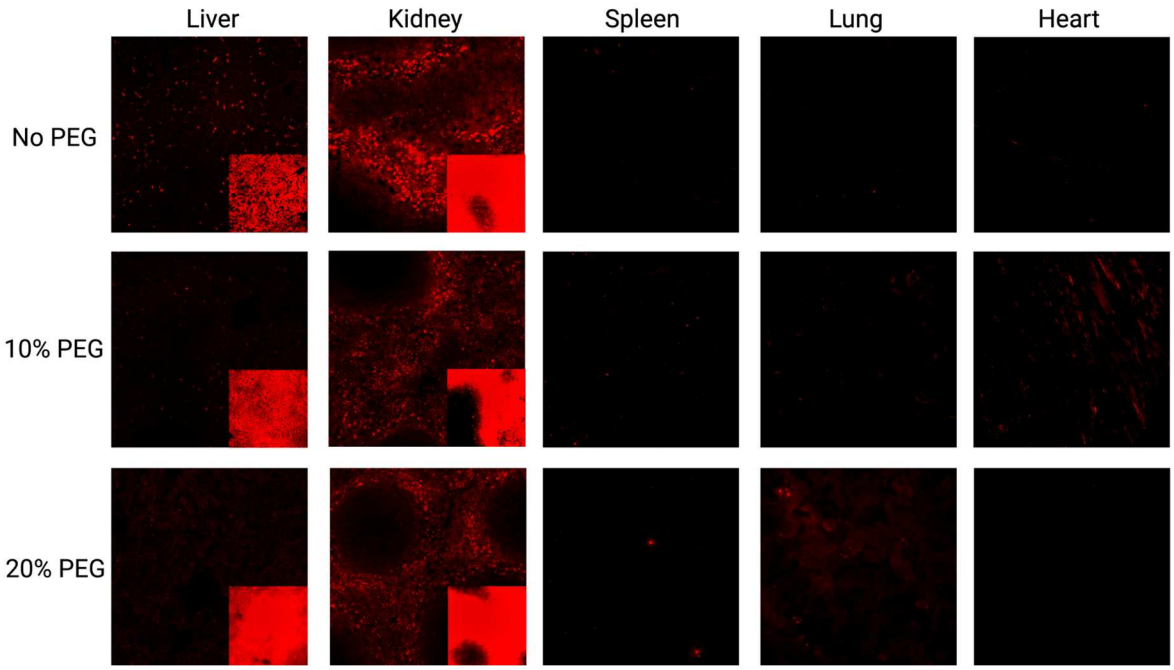

Figure 7. in vivo biodistribution study of PEGylated PLGA particles off-target organs. PEG-PLGA Nps are seen in red. Images were taken at 20x magnification. The inset seen in the Liver and Kidney images are taken at the same laser intensity and exposure time as spleen, lung, and Heart images. Exposure time was decreased for the Liver and Kidneys so that images were no longer over-exposed and visual analysis of Nps accumulation could be made.

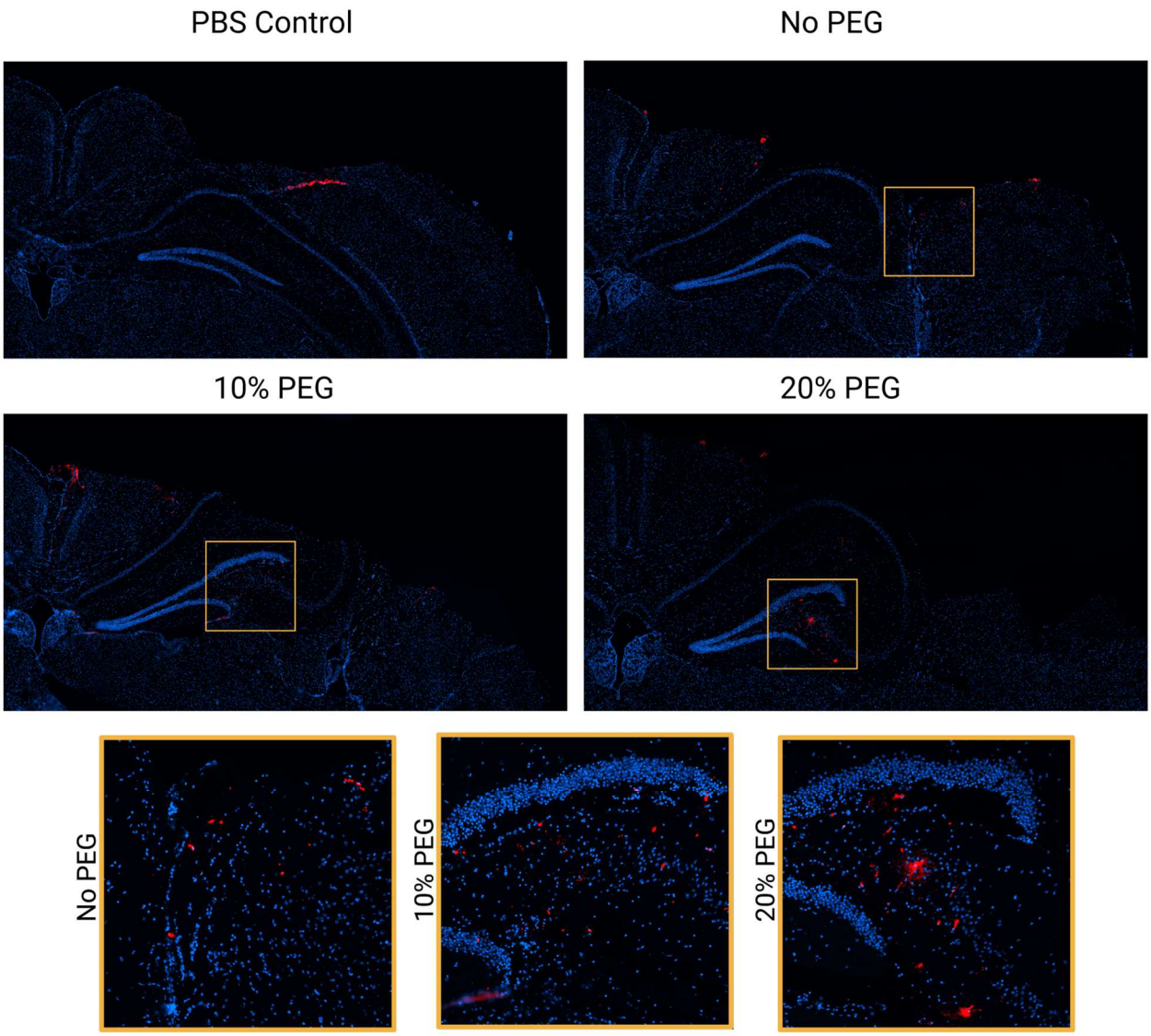

Figure 8. in vivo fluorescent spectroscopy of PEGylated PLGA particles brain accumulation. PEG-PLGA Nps are seen in red. Images were taken at 20x magnification. The region of interest (ROI) seen in quarter brain images is shown at a larger scale at the bottom of the figure. ROI displays the region of the brain with the highest Np accumulation.

Discussion

PEG-PLGA NPs of a reproducible 200 nm diameter were synthesized using a single emulsion evaporation method (**Fig. 1**). It is widely regarded that brain accumulation of Nps is highest when less than 200nm, preferably closer to 100 nm, to help particles avoid RES clearance and pass through the BBB [38]. Therefore, a size of 200 nm was targeted for this study to maximize the drug loading capabilities of the nanoparticles synthesized. It is also difficult to reliably and accurately produce PLGA NPs with00 nm using single emulsion synthesis [32]. For these reasons, PLGA-NPs with 200 nm diameter were made and characterized as having a 55% encapsulation efficiency and 2% loading capacity. It should be noted that both EE and LC decreased as PEG concentrations increased. This trend is presumably due to the self-assembly nature of hydrophobic PLGA NP becoming unstable as more hydrophilic PEG is added to the formulation.

NAC has shown neuroprotective potential and is a therapeutic drug candidate for TBI treatment but suffers from low bioavailability; this made NAC the ideal candidate for Np encapsulation. NAC-loaded PLGA NPs were also synthesized to test the feasibility of a hydrophilic drug in PLGA through the double emulsion synthesis method. The average diameter of NAC-loaded PLGA NPs was similar to PEG-PLGA NPs at ~200 nm (**Fig. 2**). However, NAC-loaded particles' encapsulation efficiency and loading capacity were greatly reduced due to the unfavorable hydrophobic encapsulation conditions during the PLGA NP synthesis [44]. Potential strategies to increase NAC encapsulation efficiency and drug load all center around attempting to make NAC more hydrophobic or the PLGA using during synthesis more hydrophilic [59]. You can attempt to make NAC more hydrophobic by reducing the pH that the synthesis takes place. PLGA becomes more hydrophilic when the polymer is acid terminated

versus ester terminated. The most promising alternative is to increase the hydrophobicity of NAC with a calcium salt that acts as a positively charged anchor within the PLGA NPs formed so that NAC has something to hold it within the nanoparticle [60]. This prevents the immediate defusal out of the NP due to a strong concentration gradient formed by the surrounding aqueous environment that the PLGA Nps are surrounded in until hardening is complete.

FRET-PLGA Np were created to characterize the dye release profile from PEG-PLGA NP (**Fig. 3**). Dye release was first characterized in situ, where a biphasic dye release profile was observed. Roughly ~8% of loaded dye was released within the first 24 hours of incubation in Situ (**Fig. 4**). Dye release then substantially decreased over the next 20 days resulting in only a ~20% dye release in the PBS pH 5.8 condition indicating that dye release becomes stable and dependent on PLGA degradation after initial burst release is completed (**Fig. 5**). The initial burst release seen in the first 24 hours is likely due to dye attached to the particle's surface and not encapsulated within the center of the particle [56]. Dye release was then characterized in vitro to better understand how PEG-PLGA Np degradation would be affected by the presence of lysosomal conditions (**Fig. 6**). From the qualitative imaging analysis, it can be determined that significant dye release has occurred within a 90 hour incubation time. However, some FRET signal is present at thr 90 hour time point, indicating that PEG-PLGA Nps are not fully degraded. Nevertheless, this is promising preliminary evidence that these PEG-PLGA NPs will be able to maintain sustained drug release in vivo for 1-2 weeks. Future work will include quantitative analysis using flow cytometry.

One of the most significant limitations in nanoparticle aided drug delivery is clearance by the RES through opsonization, and the size of the NPs influences clearance and distribution [39]. When Np size exceeds 100 nm, the pharmacokinetic and biodistribution properties significantly

change, and they are detected in blood and organs like the spleen, liver, and kidneys. The in vivo biodistribution data shown in (**Fig. 7&8**) show that PEGylating PLGA nanoparticles can help to reduce their RES clearance even with larger NPs at 200 nm in size. The addition of PEG increases the blood circulation time and allows for more effective passive accumulation of nanoparticles in the target injured brain hemisphere after TBI [38], [45], [46]. Therefore, extended in vivo time points between injection and perfusion should be examined to determine if PEG-PLGA NPs continue to accumulate as long as the BBB remains permeable after TBI. Peak accumulation of bare PLGA NPs typically occurs around one h after injection, so there should be no increased accumulation of No PEG samples when looking at longer time points [39]. However, the PEGylated particles experience increased blood-circulation times and should therefore accumulate within the brain past the 1-2 h mark as long as they remain in circulation. The blood half-life of these PEG-PLGA NPs should also be determined to understand when peak accumulation will occur.

A limitation that should be addressed in future design optimization studies is that when PLGA degrades, it tends to produce acidic byproducts that can decrease the pH of the surrounding microenvironment. It has long been recognized that a low pH can exist in PLGA delivery systems during incubation due to acidic polymer impurities and the build-up of acidic polymer degradation products [61], [62]. This can be especially a concern in the brain because while the human brain frequently changes acidity, with spikes from time to time due to carbon dioxide gas release after the break down of glucose, these fluctuations are fleeting, and the overall chemistry in healthy brains remains relatively neutral [63]. If the brain microenvironment is exposed to a decrease in pH for an extended time, it can mimic hypoxia conditions leading to autophagy and ROS production [64]. Therefore, future optimizations should be done to ensure

that these PEG-PLGA Nps do not significantly alter the brain microenvironment's pH significantly, which we do not expect due to the relatively small amount present in the brain and the week's long degradation half-life [65]. If it is determined that the degradation of PLGA creates acidic byproducts in harmful quantities for the brain, one possible alternative to look into could be the addition of titania to the NP formulation [61]. It has been found that the incorporation of titania dispersed nanoparticles into PLGA is a successful way to decrease the harmful change in pH commonly associated with PLGA degradation [66]. Moreover, studies have shown that low doses of 10 mg/kg of titania of TiO2 added to the brain had no measurable toxicity [61].

Conclusion

In conclusion, this thesis establishes a method for reproducing PEG-PLGA NPs with high encapsulation efficiencies and loading capacities using a single emulsion-evaporation synthesis method. Furthermore, PEG-PLGA NPs are stable in aqueous suspension, exhibiting sustained drug release over that time. Finally, PEGylated PLGA nanoparticles accumulate predominately near the injury region after CCI injury in mice. The addition of PEG to PLGA nanoparticles leads to reduced accumulation in RES filtration organs such as the liver and kidney. Indicating that the circulation time of PEGylated particles has been increased and can passively target the brain for a longer duration of time than bare PLGA Nps can. Detailed studies on the biodistribution of each Np, their blood half-life, and their total accumulation per brain tissue are yet to be addressed. However, the work presented here provides the groundwork for NP delivery after TBI. Therefore, a better understanding of NP accumulation will facilitate effective utilization of the BBB breakdown and help illuminate potential active targeting candidates for increased NP brain accumulation.

References

[1] D. J. Thurman, C. Alverson, D. Browne, K.A. Dunn, J. Guerrero, R. Johnson, V. Johnson, J. Langlois, D. Pilkey, J. E. Sniezek, S. Toal, "Traumatic Brain Injury in the United States: A Report to Congress," Dec. 1999.

[2] A. A. Hyder, C. A. Wunderlich, P. Puvanachandra, G. Gururaj, and O. C. Kobusingye, "The impact of traumatic brain injuries: A global perspective," IOS Press, 2007.

[3] M. C. Dewan, A. Rattani, S. Gupta, R. E. Baticulon, Y. C. Hung, M. Punchak, A. Agrawal, A. O. Adeleye, M. G. Shrime, A. M. Rubiano, J. V. Rosenfeld, K. B. Park, "Estimating the global incidence of traumatic brain injury," *Journal of Neurosurgery*, vol. 130, no. 4, pp. 1080–1097, Apr. 2019, doi: 10.3171/2017.10.JNS17352.

[4] D. of Health, H. Services, and C. for Disease Control, "Centers for Disease Control and Prevention Prevention and Control SURVEILLANCE REPORT Surveillance Report of Traumatic Brain Injury-related Emergency Department Visits, Hospitalizations, and Deaths TBI: SURVEILLANCE REPORT ACKNOWLEDGEMENTS." [Online]. Available: www.cdc.gov/TraumaticBrainInjury

[5] F. Rusciano, R. Schurch, "THE GLOBAL BURDEN OF DISEASE." World Health Organization Library Cataloguing-in-Publication Data. ISBN 978 92 4 156371 0. 2004.

[6] D. J. Loane and A. I. Faden, "Neuroprotection for traumatic brain injury: Translational challenges and emerging therapeutic strategies," *Trends in Pharmacological Sciences*, vol. 31, no. 12. pp. 596–604, Dec. 2010. doi: 10.1016/j.tips.2010.09.005.

[7] A. Giustini, C. Pistarini, and C. Pisoni, "Traumatic and nontraumatic brain injury."

[8] M. Majdan, W. Mauritz, A. Brazinova, M. Rusnak, J. Leitgeb, I. Janciak, I. Wilbacher, "Severity and outcome of traumatic brain injuries (TBI) with different causes of injury," *Brain Injury*, vol. 25, no. 9, pp. 797–805, 2011, doi: 10.3109/02699052.2011.581642.

[9] K. E. Saatman, A. C. Duhaime, R. Bullock, A. I. R. Maas, A. Valadka, G. T. Manley, "Classification of traumatic brain injury for targeted therapies," in *Journal of Neurotrauma*, Jul. 2008, vol. 25, no. 7, pp. 719–738. doi: 10.1089/neu.2008.0586.

[10] by Springer-Verlag, B. J. H Adams, and T. A. Gennarelli, "Head Injury in Man and Experimental Animals: Neuropathology," 1983.

[11] J. Lier, B. Ondruschka, I. Bechmann, and J. Dreßler, "Fast microglial activation after severe traumatic brain injuries," *International Journal of Legal Medicine*, vol. 134, no. 6, pp. 2187–2193, Nov. 2020, doi: 10.1007/s00414-020-02308-x.

[12] C. K. Donat, G. Scott, S. M. Gentleman, and M. Sastre, "Microglial activation in traumatic brain injury," *Frontiers in Aging Neuroscience*, vol. 9, no. JUN. Frontiers Media S.A., Jun. 28, 2017. doi: 10.3389/fnagi.2017.00208.

[13] A. Kumar, B. A. Stoica, B. Sabirzhanov, M. P. Burns, A. I. Faden, and D. J. Loane, "Traumatic brain injury in aged animals increases lesion size and chronically alters microglial/macrophage classical and alternative activation states," *Neurobiology of Aging*, vol. 34, no. 5, pp. 1397–1411, May 2013, doi: 10.1016/j.neurobiolaging.2012.11.013.

[14] J. M. Zhou, S. S. Gu, W. H. Mei, J. Zhou, Z. Z. Wang, and W. Xiao, "Ginkgolides and bilobalide protect BV2 microglia cells against OGD/reoxygenation injury by inhibiting TLR2/4 signaling pathways," *Cell Stress and Chaperones*, vol. 21, no. 6, pp. 1037–1053, Nov. 2016, doi: 10.1007/s12192-016-0728-y.

[15] F. Zhang, E. Nance, Y. Alnasser, R. Kannan, and S. Kannan, "Microglial migration and interactions with dendrimer nanoparticles are altered in the presence of neuroinflammation," *Journal of Neuroinflammation*, vol. 13, no. 1, Mar. 2016, doi: 10.1186/s12974-016-0529-3.

[16] R. Fong, S. Konakondla, C. M. Schirmer, and M. Lacroix, "Surgical interventions for severe traumatic brain injury," *Journal of Emergency and Critical Care Medicine*, vol. 1, no. 10, pp. 28–28, Oct. 2017, doi: 10.21037/jeccm.2017.09.03.

[17] J. A. Kudryashev, L. E. Waggoner, H. T. Leng, N. H. Mininni, and E. J. Kwon, "An Activity-Based Nanosensor for Traumatic Brain Injury," *ACS Sensors*, vol. 5, no. 3, pp. 686–692, Mar. 2020, doi: 10.1021/acssensors.9b01812.

[18] N. Stocchetti, F. S. Taccone, G. Citerio, P. E. Pepe, P. D. Roux, M. Oddo, K. H. Polderman, R. D. Stevens, W. Barsan, A. I. Mass, G. Meyfroidt, M. J. Bell, "Neuroprotection in acute brain injury: An up-to-date review," *Critical Care*, vol. 19, no. 1. BioMed Central Ltd., Apr. 21, 2015. doi: 10.1186/s13054-015-0887-8.

[19] Y. J. Kim, "The Impact of Time from ED Arrival to Surgery on Mortality and Hospital Length of Stay in Patients With Traumatic Brain Injury," *Journal of Emergency Nursing*, vol. 37, no. 4, pp. 328–333, Jul. 2011, doi: 10.1016/j.jen.2010.04.017.

[20] S. Y. Ng and A. Y. W. Lee, "Traumatic Brain Injuries: Pathophysiology and Potential Therapeutic Targets," *Frontiers in Cellular Neuroscience*, vol. 13. Frontiers Media SA, Nov. 27, 2019. doi: 10.3389/fncel.2019.00528.

[21] M. E. Hoffer, C. Balaban, M. D. Slade, J. W. Tsao, and B. Hoffer, "Amelioration of Acute Sequelae of Blast Induced Mild Traumatic Brain Injury by N-Acetyl Cysteine: A Double-Blind, Placebo Controlled Study," *PLoS ONE*, vol. 8, no. 1, Jan. 2013, doi: 10.1371/journal.pone.0054163.

[22] D. G. Stein, "Embracing failure: What the Phase III progesterone studies can teach about TBI clinical trials," *Brain Injury*, vol. 29, no. 11. Taylor and Francis Ltd, pp. 1259–1272, Sep. 19, 2015. doi: 10.3109/02699052.2015.1065344.

[23] I. Camacho-Arroyo, G. P6rez-Palacios, A. M. Pasapera, and M. A. Cerb6n, "Intracellular Progesterone Receptors are Differentially Regulated by Sex Steroid Hormones in the Hypothalamus and the Cerebral Cortex of the Rabbit," 1994.

[24] D. W. Wright, S. D. Yeatts, R. Silbergleit, Y. Y. Palesch, V. S. Hertzberg, M. Frankel, F. C. Goldstein, A. F. Caveney, "Very Early Administration of Progesterone for Acute Traumatic Brain Injury," *New England Journal of Medicine*, vol. 371, no. 26, pp. 2457–2466, Dec. 2014, doi: 10.1056/nejmoa1404304.

[25] S. Margulies, R. Hicks, "Combination Therapies for Traumatic Brain Injury: Prospective Considerations The Combination Therapies for Traumatic Brain Injury Workshop Leaders*", doi: 10.1089=neu.2008.0794.

[26] R. M. Kandell, L. E. Waggoner, and E. J. Kwon, "Nanomedicine for Acute Brain Injuries: Insight from Decades of Cancer Nanomedicine," *Molecular Pharmaceutics*, vol. 18, no. 2. American Chemical Society, pp. 522–538, Feb. 01, 2021. doi: 10.1021/acs.molpharmaceut.0c00287.

[27] R. Vink and A. J. Nimmo, "Multifunctional Drugs for Head Injury."

[28] B. J. Hoffer, C. G. Pick, M. E. Hoffer, R. E. Becker, Y. H. Chiang, and N. H. Greig, "Repositioning drugs for traumatic brain injury - N-acetyl cysteine and Phenserine," *Journal of Biomedical Science*, vol. 24, no. 1. BioMed Central Ltd., Sep. 09, 2017. doi: 10.1186/s12929-017-0377-1.

[29] K. Eakin, R. B. Goldstein, C. G. Pick, O. Zindel, C. D. Balaban, M. E. Hoffer, M. Lockwood, J. Miller, B. J. Hoffer, "Efficacy of N-acetyl cysteine in traumatic brain injury," *PLoS ONE*, vol. 9, no. 4, Apr. 2014, doi: 10.1371/journal.pone.0090617.

[30] S. L. Dix and J. P. Aggleton, "Extending the spontaneous preference test of recognition: evidence of object-location and object-context recognition," 1999.

[31] G. Chen, J. Shi, Z. Hu, and C. Hang, "Inhibitory effect on cerebral inflammatory response following traumatic brain injury in rats: A potential neuroprotective mechanism of N-Acetylcysteine," *Mediators of Inflammation*, vol. 2008, 2008, doi: 10.1155/2008/716458.

[32] G. D. Mahumane, P. Kumar, V. Pillay, and Y. E. Choonara, "Repositioning n-acetylcysteine (NAC): Nac-loaded electrospun drug delivery scaffolding for potential neural tissue engineering application," *Pharmaceutics*, vol. 12, no. 10, pp. 1–19, Oct. 2020, doi: 10.3390/pharmaceutics12100934.

[33] V. I. Lushchak, "Glutathione Homeostasis and Functions: Potential Targets for Medical Interventions," *Journal of Amino Acids*, vol. 2012, pp. 1–26, Feb. 2012, doi: 10.1155/2012/736837.

[34] E. F. Ellis, L. Y. Dodson, and R. J. Police, "Restoration of cerebrovascular responsiveness to hyperventilation by the oxygen radical scavenger n-acetylcysteine following experimental traumatic brain injury," 1991.

[35] R. Diaz-Arrastia, P. M. Kochanek, P. Bergold, K. Kenney, C. E. Marx, J. B. Grimes, Y. Loh, G. E. Adam, D. Oskvig, "Pharmacotherapy of traumatic brain injury: State of the science and the road forward: Report of the department of defense neurotrauma pharmacology workgroup," *Journal of Neurotrauma*, vol. 31, no. 2. pp. 135–158, Jan. 15, 2014. doi: 10.1089/neu.2013.3019.

[36] D. Chenthamara, S. Subramaniam, S. G. Ramakrishnan, S. Krishnaswamy, M. M. Essa, F. H. Lin, M. W. Qoronfleh, "Therapeutic efficacy of nanoparticles and routes of administration," *Biomaterials Research*, vol. 23, no. 1. BioMed Central Ltd., Nov. 21, 2019. doi: 10.1186/s40824-019-0166-x.

[37] B. A. Bony and F. M. Kievit, "A role for nanoparticles in treating traumatic brain injury," *Pharmaceutics*, vol. 11, no. 9. MDPI AG, Sep. 01, 2019. doi: 10.3390/pharmaceutics11090473.

[38] B. J. Boyd, A. Galle, M. Daglas, J. v. Rosenfeld, and R. Medcalf, "Traumatic brain injury opens blood-brain barrier to stealth liposomes via an enhanced permeability and retention (EPR)-like effect," *Journal of Drug Targeting*, vol. 23, no. 9, pp. 847–853, Oct. 2015, doi: 10.3109/1061186X.2015.1034280.

[39] V. N. Bharadwaj, J. Lifshitz, P. D. Adelson, V. D. Kodibagkar, and S. E. Stabenfeldt, "Temporal assessment of nanoparticle accumulation after experimental brain injury: Effect of particle size," *Scientific Reports*, vol. 6, Jul. 2016, doi: 10.1038/srep29988.

[40] J. Shi, P. W. Kantoff, R. Wooster, and O. C. Farokhzad, "Cancer nanomedicine: progress, challenges and opportunities," *Nature Reviews Cancer*, vol. 17, no. 1. Nature Publishing Group, pp. 20–37, Jan. 01, 2017. doi: 10.1038/nrc.2016.108.

[41] V. N. Bharadwaj, D. T. Nguyen, V. D. Kodibagkar, and S. E. Stabenfeldt, "Nanoparticle-Based Therapeutics for Brain Injury," *Advanced Healthcare Materials*, vol. 7, no. 1, Jan. 2018, doi: 10.1002/adhm.201700668.

[42] J. S. Suk, Q. Xu, N. Kim, J. Hanes, and L. M. Ensign, "PEGylation as a strategy for improving nanoparticle-based drug and gene delivery," *Advanced Drug Delivery Reviews*, vol. 99. Elsevier BV, pp. 28–51, Apr. 01, 2016. doi: 10.1016/j.addr.2015.09.012.

[43] R. Dinarvand, T. Sadat, J. Kashi, S. Eskandarion, M. E. Manesh, S. Mahmoud, A. Marashi, N. Samadi, S. M. Fatemi, F. Atyabi, S. Eshraghi, "Improved drug loading and

antibacterial activity of minocycline-loaded PLGA nanoparticles prepared by solid/oil/water ion pairing method," *International Journal of Nanomedicine*, p. 221, Jan. 2012, doi: 10.2147/ijn.s27709.

[44] N. P. Murphy and K. J. Lampe, "Fabricating PLGA microparticles with high loads of the small molecule antioxidant N-acetylcysteine that rescue oligodendrocyte progenitor cells from oxidative stress," *Biotechnology and Bioengineering*, vol. 115, no. 1, pp. 246–256, Jan. 2018, doi: 10.1002/bit.26443.

[45] D. Gonzalez-Carter, X. Liu, T. A. Tockary, A. Dirisala, K. Toh, Y. Anraku, K. Kataoka, "Targeting nanoparticles to the brain by exploiting the blood-brain barrier impermeability to selectively label the brain endothelium", doi: 10.1073/pnas.2002016117/-/DCSupplemental.

[46] A. Chodobski, B. J. Zink, and J. Szmydynger-Chodobska, "Blood-Brain Barrier Pathophysiology in Traumatic Brain Injury," *Translational Stroke Research*, vol. 2, no. 4. pp. 492–516, Dec. 2011. doi: 10.1007/s12975-011-0125-x.

[47] W. Huang and C. Zhang, "Tuning the Size of Poly(lactic-co-glycolic Acid) (PLGA) Nanoparticles Fabricated by Nanoprecipitation," *Biotechnology Journal*, vol. 13, no. 1, Jan. 2018, doi: 10.1002/biot.201700203.

[48] R. Lball, P. Bajaj, and K. A. Whitehead, "Achieving long-term stability of lipid nanoparticles: Examining the effect of pH, temperature, and lyophilization," *International Journal of Nanomedicine*, vol. 12, pp. 305–315, 2017, doi: 10.2147/IJN.S123062.

[49] S. D'Souza, "A Review of In Vitro Drug Release Test Methods for Nano-Sized Dosage Forms ," *Advances in Pharmaceutics*, vol. 2014, pp. 1–12, Nov. 2014, doi: 10.1155/2014/304757.

[50] E. M. Elmowafy, M. Tiboni, and M. E. Soliman, "Biocompatibility, biodegradation and biomedical applications of poly(lactic acid)/poly(lactic-co-glycolic acid) micro and nanoparticles," *Journal of Pharmaceutical Investigation*, vol. 49, no. 4. Springer Netherlands, pp. 347–380, Jul. 01, 2019. doi: 10.1007/s40005-019-00439-x.

[51] J. R. Kanwar, X. Sun, V. Punj, B. Sriramoju, R. R. Mohan, S. F. Zhou, A. Chauhan, R. K. Kanwar, "Nanoparticles in the treatment and diagnosis of neurological disorders: Untamed dragon with fire power to heal," *Nanomedicine: Nanotechnology, Biology, and Medicine*, vol. 8, no. 4. pp. 399–414, May 2012. doi: 10.1016/j.nano.2011.08.006.

[52] S. R. Mudshinge, A. B. Deore, S. Patil, and C. M. Bhalgat, "Nanoparticles: Emerging carriers for drug delivery," *Saudi Pharmaceutical Journal*, vol. 19, no. 3. pp. 129–141, Jul. 2011. doi: 10.1016/j.jsps.2011.04.001.

[53] X. Wu, J. Zhou, and T. R. Patel, "Generation of ultra-small PLGA nanoparticles by sequential centrifugation," in *Methods in Molecular Biology*, vol. 1831, Humana Press Inc., 2018, pp. 17–24. doi: 10.1007/978-1-4939-8661-3_2.

[54] E. Swider, O. Koshkina, J. Tel, L. J. Cruz, I. J. M. de Vries, and M. Srinivas, "Customizing poly(lactic-co-glycolic acid) particles for biomedical applications," *Acta Biomaterialia*, vol. 73. Acta Materialia Inc, pp. 38–51, Jun. 01, 2018. doi: 10.1016/j.actbio.2018.04.006.

[55] T. Eickner, T. Reske, S. Illner, K. P. Schmitz, D. P. Martin, and N. Grabow, "Fast parallel quantification of dual drug systems via UV-VIS spectrometry – A case study with antibiotic substances," *Current Directions in Biomedical Engineering*, vol. 3, no. 2, pp. 375–378, Sep. 2017, doi: 10.1515/cdbme-2017-0078.

[56] H. Chen, S. Kim, W. He, H. Wang, P. S. Low, K. Park, J. X. Cheng, "Fast release of lipophilic agents from circulating PEG-PDLLA micelles revealed by in vivo Förster resonance energy transfer imaging," *Langmuir*, vol. 24, no. 10, pp. 5213–5217, May 2008, doi: 10.1021/la703570m.

[57] S. Y. Fam, C. F. Chee, C. Y. Yong, K. L. Ho, A. R. Mariatulqabtiah, and W. S. Tan, "Stealth coating of Nanoparticles in drug-delivery systems," *Nanomaterials*, vol. 10, no. 4. MDPI AG, Apr. 01, 2020. doi: 10.3390/nano10040787.

[58] E. Swider, S. Maharjan, K. Houkes, N. Koen, C. Figdor, M. Srinivas, O. Tagit, "Förster Resonance Energy Transfer-Based Stability Assessment of PLGA Nanoparticles in Vitro and in Vivo," *ACS Applied Bio Materials*, vol. 2, no. 3, pp. 1131–1140, Mar. 2019, doi: 10.1021/acsabm.8b00754.

[59] R. Lancheros, C. A. Guerrero, and R. D. Godoy-Silva, "Improvement of N-Acetylcysteine Loaded in PLGA Nanoparticles by Nanoprecipitation Method," *Journal of Nanotechnology*, vol. 2018, 2018, doi: 10.1155/2018/3620373.

[60] K. Goud, H. Desai, S. R. Mallery, and S. P. Schwendeman, "Formulation and Characterization of Injectable Poly(DL-lactide-co-glycolide) Implants Loaded with N-Acetylcysteine, a MMP Inhibitor," 2008.

[61] H. Liu, E. B. Slamovich, and T. J. Webster, "Less harmful acidic degradation of poly(lactic-co-glycolic acid) bone tissue engineering scaffolds through titania nanoparticle addition," 2006.

[62] A. G. Ding and S. P. Schwendeman, "Acidic microclimate pH Distribution in PLGA microspheres monitored by confocal laser scanning microscopy," *Pharmaceutical Research*, vol. 25, no. 9, pp. 2041–2052, Sep. 2008, doi: 10.1007/s11095-008-9594-3.

[63] H. Hagihara, V. S. Catts, Y. Katayama, H. Shoji, T. Takagi, F. L. Huang, A. Nakao, Y. Mori, K. P. Huang, S. Ishii, I. A. Graef, K. I. Nakayama, C. S. Weickert, T. Miyakawa, "Decreased Brain pH as a Shared Endophenotype of Psychiatric Disorders," *Neuropsychopharmacology*, vol. 43, no. 3, pp. 459–468, Feb. 2018, doi: 10.1038/npp.2017.167.

[64] R. Chen, U. H. Lai, L. Zhu, A. Singh, M. Ahmed, and N. R. Forsyth, "Reactive oxygen species formation in the brain at different oxygen levels: The role of hypoxia inducible factors," *Frontiers in Cell and Developmental Biology*, vol. 6, no. OCT. Frontiers Media S.A., Oct. 10, 2018. doi: 10.3389/fcell.2018.00132.

[65] R. H. Ansary, M. B. Awang, and M. M. Rahman, "Biodegradable poly(D,L-lactic-co-glycolic acid)-based micro/nanoparticles for sustained release of protein drugs - A review," *Tropical Journal of Pharmaceutical Research*, vol. 13, no. 7. University of Benin, pp. 1179–1190, 2014. doi: 10.4314/tjpr.v13i7.24.

[66] X. Jia, S. Wang, L. Zhou, and L. Sun, "The Potential Liver, Brain, and Embryo Toxicity of Titanium Dioxide Nanoparticles on Mice," *Nanoscale Research Letters*, vol. 12, 2017, doi: 10.1186/s11671-017-2242-2.